

Remarkable Interplay of Redox States and Conformational Changes in a Sterically Crowded, Cross-Conjugated Tetrathiafulvalene Vinyllog

Samia Amriou,^[a] Igor F. Perepichka,^[a] Andrei S. Batsanov,^[a] Martin R. Bryce,^{*[a]} Concepció Rovira,^[b] and José Vidal-Gancedo^[b]

Abstract: Derivatives of 9-[2-(1,3-dithiol-2-ylidene)ethylidene]thioxanthenes have been synthesized using Horner–Wadsworth–Emmons reactions of (1,3-dithiol-2-yl)phosphonate reagents with thioxanthen-9-ylidene-acetaldehyde (**5**). Further reactions lead to the sterically crowded cross-conjugated “vinyllogous tetrathiafulvalene” derivative 9-[2,3-bis-(4,5-dimethyl-1,3-dithiol-2-ylidene)-propylidene]thioxanthenes (**10**). X-ray crystallography, solution electrochemistry, optical spectroscopy, spectroelectrochemistry, and simultaneous electrochemistry and electron paramagnetic resonance spectroscopy, combined with theoretical calculations performed at the B3LYP/6-31G(d) level, elucidate the interplay of the electronic and structural properties in these mole-

cules. For compound **10**, multistage redox behavior is observed: the overall electrochemical process can be represented by $10 \rightarrow 10^{+\cdot} \rightarrow 10^{2+} \rightarrow 10^{4+}$ with good reversibility for the $10 \rightarrow 10^{+\cdot} \rightarrow 10^{2+}$ transformations. At the tetracation stage there is the maximum gain in aromaticity at the dithiolium and thioxanthenium rings. Theory predicts that for **10**, $10^{+\cdot}$, and 10^{2+} the *trans* isomers are more stable than the *cis* isomers (by ca. 2–18 kJ mol⁻¹), whereas for 10^{4+} the *cis* isomer becomes more stable than the *trans* isomer (by ca. 25 kJ mol⁻¹) [*trans* and *cis* refer to the

arrangement of the two dithiole moieties with respect to the central =C(R)–C(H)= fragment]. These data explain the detection in cyclic voltammograms of both *trans* and *cis* isomers of **10** and $10^{+\cdot}$ during the reduction of 10^{4+} at fast scan rates (>100 mVs⁻¹) when the *cis*–*trans* isomerization is not completed within the timescale of the experiment. The X-ray structure of the charge-transfer complex (CTC) of **10** with 2,4,5,7-tetranitrofluorene-9-dicyanomethylenefluorene (DTeF) [stoichiometry: $10^{+\cdot} \cdot (\text{DTeF})_2^{-} \cdot 2\text{PhCl}$] reveals a twisted conformation of $10^{+\cdot}$ (driven by the bulky thioxanthenes moiety) and provides a very rare example of segregated stacking of a fluorene acceptor in a CTC.

Keywords: charge transfer • cross-conjugation • dendralene • electrochemistry • sulfur heterocycles

Introduction

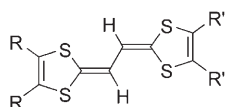
The 1,3-dithiol-2-ylidene unit has been extensively modified to provide analogues of the famous π -electron donor tetrathiafulvalene (TTF). Derivatives with one 1,3-dithiol-2-ylidene group attached to aromatic/heteroaromatic frameworks,^[1] are poorer electron donors than TTF. On the other hand, vinyllogous bis(1,3-dithioles) **1**^[2–8] have attracted more attention, because they are stronger electron donors with reduced on-site Coulombic repulsion. Consequently they possess a smaller difference (ΔE) between the first and second oxidation potentials, which represent the sequential formation of cation radical and dication species. For derivatives with longer conjugated spacers (both olefinic^[2,6] and acetylenic^[9]) the terminal dithiole units reach a separation distance at which they behave as independent redox centers under electrochemical conditions and the waves coalesce into a single, two-electron process. A different set of deriva-

[a] Dr. S. Amriou, Dr. I. F. Perepichka,* Dr. A. S. Batsanov, Prof. M. R. Bryce
Department of Chemistry and
Centre for Molecular and Nanoscale Electronics
University of Durham, Durham DH1 3LE (UK)
Fax: (+44)191-384-4737
E-mail: m.r.bryce@durham.ac.uk

[b] Prof. C. Rovira, Dr. J. Vidal-Gancedo
Institut de Ciència de Materials de Barcelona (CSIC)
Campus Universitari, 08193 Bellaterra, Catalonia (Spain)

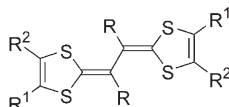
[*] On leave from L. M. Litvinenko
Institute of Physical Organic and Coal Chemistry
National Academy of Sciences of Ukraine
Donetsk 83114 (Ukraine)

Supporting information for this article is available on the WWW under <http://www.chemistry.org> or from the authors. It contains cyclic voltammetry, spectroelectrochemistry and DFT calculations data for compounds **8** and **10**; UV/Vis/NIR electron absorption spectra of charge transfer complex of **10** with DTeF and crystal packing diagrams of $10 \cdot (\text{DTeF})_2 \cdot 2\text{PhCl}$.



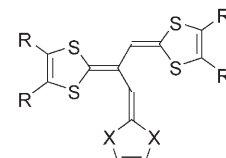
1a–n,

- a, R = R' = H
- b, R = R' = Me
- c, R = R' = SMe
- d, R = R' = CO₂Me
- e, 2R = 2R' = -SCH₂CH₂S-
- f, 2R = 2R' = -SCH₂CH₂CH₂S-
- g, 2R = 2R' = -(CH=CH)₂-
- h, R = SMe; R' = Me
- i, R = SMe; R' = SeMe
- j, R = H; 2R' = -SCH₂CH₂CH₂S-
- k, R = Me; 2R' = -SCH₂CH₂CH₂S-
- l, R = SMe; 2R' = -SCH₂CH₂CH₂S-
- m, R = H; 2R' = -SCH₂CH₂S-
- n, R = Me; 2R' = -SCH₂CH₂S-



2a–i,

- a, R = Ph or substituted phenyls; R¹ = Me; R² = SMe
- b, R = Me; (R¹ + R²) = -SCH₂CH₂S-
- c, R = Ph or substituted phenyls; (R¹ + R²) = -SCH₂CH₂S-
- d, R = 1-naphthyl; (R¹ + R²) = -SCH₂CH₂S-
- e, R = Me; (R¹ + R²) = -(CH=CH)₂-
- f, R = Ph or substituted phenyls; (R¹ + R²) = -(CH=CH)₂-
- g, R = 1-naphthyl; (R¹ + R²) = -(CH=CH)₂-
- h, R = 1-pyrenyl; (R¹ + R²) = -(CH=CH)₂-
- i, R = CO₂Et, R¹ = R² = Me
- j, R = Me, R¹ = R² = Me
- k, R = CN, R¹ = R² = Me
- l, R = ferrocenyl; R¹ = R² = Me



3 X = S, Se; R = H, CO₂Me

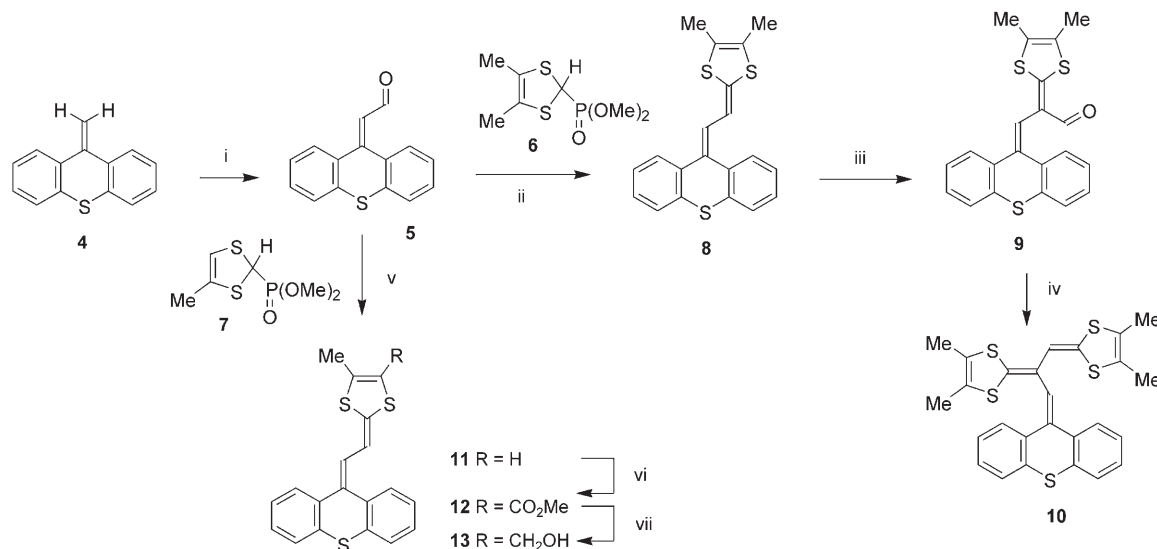
tives, which also give a two-electron wave, comprise shorter length vinylogs, in which bulky substituents (usually aryl groups, although Me and CO₂Et groups were used as well) are attached to the spacer (**2a–j**), leading to substantial conformational changes upon oxidation.^[10–12] This last set of systems provide very interesting examples of “inverted potentials”,^[13] whereas the less distorted structure **2k** (R = CN) undergoes two one-electron oxidation processes.^[12]

Another structural modification to the vinylogous scaffold, which leads to intriguing and more complex multielectron oxidation processes, involves the attachment of one or two redox-active pendant group(s). Very few derivatives of this type have been synthesized and their properties have not been explored in depth: examples are the bis(ferrocenyl) derivative **2l**^[14] and the 1,3-dithiol-2-ylidene^[15,16] and 1,3-diselenol-2-ylidene cross-conjugated dendralene systems **3**.^[17] The aim of the present work was to develop this topic

by incorporation of the 9-thioxanthene modulus into π -extended 1,3-dithiol-2-ylidene structures and to elucidate their structural, redox, and optoelectronic properties in detail. Herein we describe new conjugated vinylogous systems (e.g., **8**) and the cross-conjugated derivative **10**. We also discuss theoretical DFT studies for different oxidation states of molecules **8** and **10**, which in the latter case strongly support our interpretation of the remarkable electrochemistry observed for this compound.

Results and Discussion

Synthesis: The reaction sequence shown in Scheme 1 provided our target compounds. 9-Methylenethioxanthene (**4**) was obtained in 80% yield from thioxanthene-9-one by a Grignard reaction with methyl magnesium bromide, as de-



Scheme 1. Reagents and conditions: i) POCl₃, DMF, 0°C; then add **4**, DMF, 0°C to 60°C; ii) **6**, THF, *n*BuLi, -78°C; then add **5**, THF, -78°C to 20°C; iii) POCl₃, DMF, 0°C; then add **8**, DMF, 0°C to 60°C; iv) **6**, THF, *n*BuLi, -78°C; then add **9**, THF, -78°C to 20°C; v) **7**, THF, *n*BuLi, -78°C; then add **5**, THF, -78°C to 20°C; vi) **11**, *n*BuLi, THF, -78°C; then add ClCO₂Me, 20°C; vii) **12**, LiAlH₄, THF, -78°C to 20°C.

scribed in the literature.^[18] The reaction of **4** with phosphorus oxychloride in *N,N*-dimethylformamide (DMF) gave compound **5** in 58% yield. Reaction of **5** with the anion generated from phosphonate ester reagents **6**^[19] and **7**^[20] under Horner–Wadsworth–Emmons conditions gave the 1,3-dithiol-2-ylidene derivatives **8** and **11**, respectively, as red solids in approximately 60% yields. By analogy with the preparation of **5**, compound **9** was obtained from **8** in 95% yield. It is worth noting that this reaction is regiospecific, occurring at the methylene carbon atom attached to the more strongly electron-donating dithiole ring. The aldehyde group of compound **9** then underwent a further olefination reaction with reagent **6** to yield the dendralene product **10** as a dark red solid in 23% yield.

Access to more highly-functionalized derivatives of **11** was established by deprotonation of the hydrogen attached to the dithiole ring by using *n*-butyllithium in tetrahydrofuran (THF) at -78°C , followed by in situ trapping of the lithiated species with methyl chloroformate to give the methyl ester derivative **12** (80% yield), which was reduced with lithium aluminium hydride to the hydroxymethyl derivative **13** (70% yield).

Solution electrochemical studies: Cyclic voltammetry (CV) data for compounds **8** and **11–13**, all with only one dithiole unit, show an irreversible or quasireversible oxidation at high potentials, which is presumably a two-electron process (Figure S1 in the Supporting Information). This is typical electrochemical behavior for extended-TTF systems,^[21] which undergo a drastic change in their geometry during the oxidation due to the “inverted potentials” for the first and second single-electron oxidation steps.^[13] For extended TTFs, in which two dithiol-2-ylidene moieties are separated by a dihydro-9,10-anthracenediylidene bridge, a tremendous gain in aromaticity during the formation of the dication facilitates the two-electron transfer process. Similarly, for compounds **8** and **11–13** such a $2e^{-}$ oxidation process to yield the dication state produces an aromatic thioxanthenium cation moiety. Theoretical calculations for compound **8** reveal a large geometry change during the oxidation process $\mathbf{8} \rightarrow \mathbf{8}^{2+}$ and planarization and aromatization of the thioxanthenone moiety, thus supporting the observed electrochemical behavior (see Theoretical Calculations section).

Most intriguing electrochemical behavior was expected for compound **10**, which combines the structure of extended TTFs with an ethylene bridge (which are stronger donors than compounds **8** and **11–13** with only one dithiole moiety, and which can be oxidized in either a $2e^{-}$ process or two consecutive $1e^{-}$ processes depending on their structures and CV conditions) and a thioxanthenone-9-ylidene fragment attached to the bridge. To study the electrochemical properties of compound **10**, we performed CV experiments in both dichloromethane (CH_2Cl_2) and acetonitrile (MeCN). In CH_2Cl_2 two consecutive single-electron oxidation waves were observed (Figure 1 and Figure S2 in the Supporting Information). Both waves correspond to a reversible single-electron oxidation process, based on the difference between

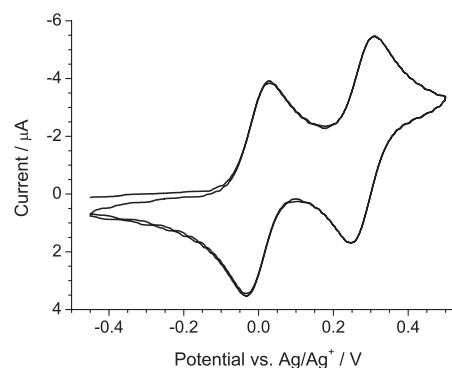


Figure 1. Cyclic voltammogram of compound **10** in CH_2Cl_2 , 0.2 M Bu_4NPF_6 , scan rate 100 mV s^{-1} (first two cycles shown).

the anodic and cathodic peak potentials ($\Delta E_{\text{pa-pc}} \sim 0.06 \text{ V}$) and currents ($i_{\text{pa}} \approx i_{\text{pc}}$), thus resulting in the radical cation ($\mathbf{10}^{\cdot+}$) and the dication ($\mathbf{10}^{2+}$) species, respectively. This electrochemical behavior is similar to that of TTF vinyllogs unsubstituted at the vinyl positions.^[2–4,7,8] For TTF vinyllogs that are symmetrically substituted in the $=\text{C}(\text{R})-\text{C}(\text{R})=$ fragment (**2a–h**), for which large conformation changes are expected upon oxidation, the situation depends on the steric and electronic effects of the substituents R, as well as on the solvent used (coalescence of the two single-electron waves was observed when CH_2Cl_2 was replaced by more polar MeCN).^[10] In the case of bulky aryl substituents ($\text{R} = o\text{-Ph}$, 1-naphthyl, 1-pyrenyl) the oxidation generally proceeds as two consecutive single-electron processes, whereas for $\text{R} = \text{Me}$ or $p\text{-Ph}$ the two redox waves coalesce, resulting in a one-step two-electron oxidation. (Decoalescence was observed for *para*-substituted phenyls with strong electron-donating groups like $\text{Me}_2\text{N-}$ or MeO- .^[5,10,11]) It should be noted that unsymmetrically substituted dendralene-type TTF vinyllogs also showed two single-electron oxidation waves.^[16,17]

On increasing the potential to $\sim 1.3 \text{ V}$ (vs. Ag/Ag^+ reference electrode), a third, partly reversible two-electron oxidation wave was observed to form the tetracation $\mathbf{10}^{4+}$ (Figure 2a). At low scan rate of 30 mV s^{-1} the overall electrochemical process can be described as $\mathbf{10} \rightarrow \mathbf{10}^{\cdot+} \rightarrow \mathbf{10}^{2+} \rightarrow \mathbf{10}^{4+}$, which on the reverse scan and on further cycling demonstrated good reversibility for the $\mathbf{10} \rightarrow \mathbf{10}^{\cdot+} \rightarrow \mathbf{10}^{2+}$ transformations. However, when the scan rate was increased to 100 mV s^{-1} , after the oxidation of **10** to $\mathbf{10}^{4+}$, an additional cathodic peak on the reverse scan was observed with an E_{pc} that is more negative than $E_{\text{pc}}^{\text{ox1}}$ (Figure 2b). Further cycling revealed the appearance of an additional reversible redox process at more negative potentials than the first oxidation $E_{1/2}^{\text{ox1}}$. This wave is clearly visible in the deconvoluted CV traces (Figure 2b). This behavior is retained, and even becomes more pronounced, when the scan rate was further increased to 300 mV s^{-1} (Figure 2c), 600, and 2000 mV s^{-1} (Figures S3 and S4 in the Supporting Information).

To understand this fascinating electrochemical behavior we considered the geometrical structure of compound **10**.

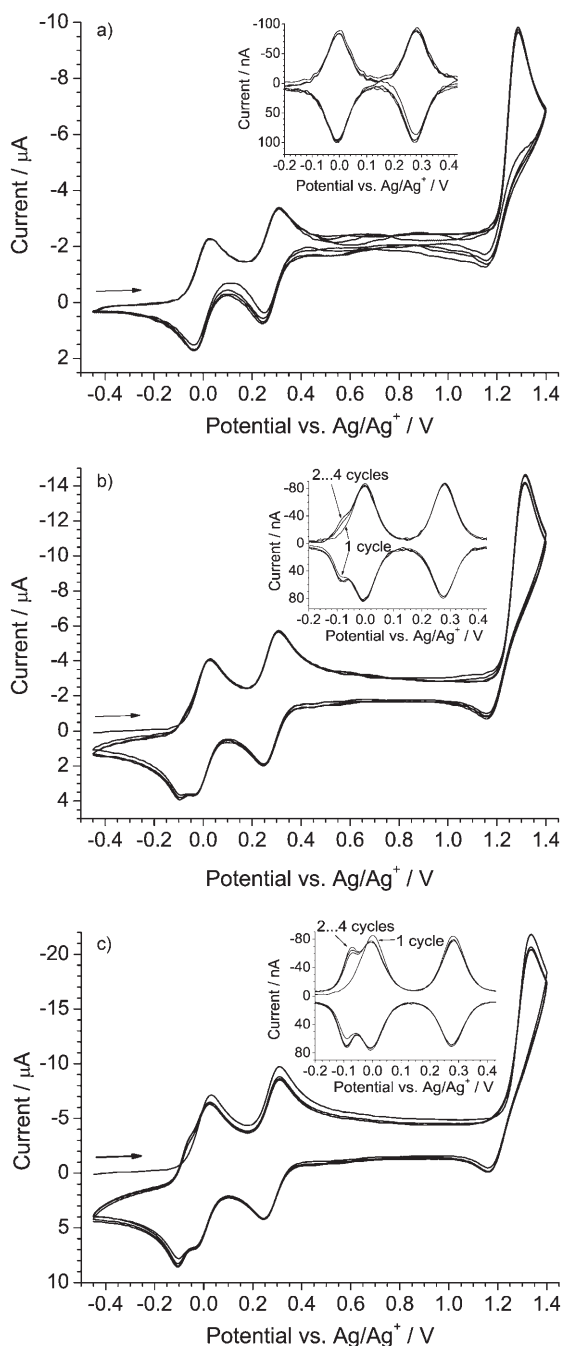
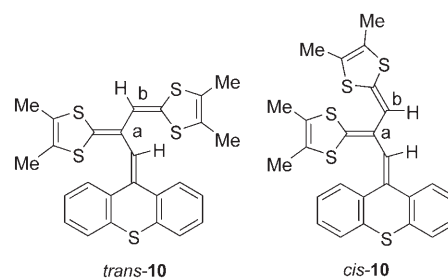


Figure 2. Cyclic voltammograms of compound **10** in CH₂Cl₂, 0.2 M Bu₄NPF₆; four consecutive scans at scan rates of a) 30, b) 100, and c) 300 mVs⁻¹. Insets show the deconvoluted CVs.

Although TTF vinylogs that are unsubstituted or symmetrically disubstituted (at the central =C(R)–C(R)= fragment) generally exist with *trans* arrangements of the dithiole moieties,^[10,11] the geometry of the unsymmetrical structure **10** can be substantially dictated by the bulky thioxanthene moiety. For example, TTF vinylogs of type **2**, in which two dithiole rings are linked through the aliphatic bridge [**2**, R = Ph or substituted phenyls; R¹ = Me; (R² + R²) = –S(CH₂)_nS–, n = 3–14] adopt a *cis* conformation of the dithiole frag-

ments.^[22] Therefore, it is not evident as to whether compound **10** exists as the *trans* or *cis* isomer.^[23] Unfortunately, crystals of **10** suitable for single-crystal X-ray diffraction analysis were not obtained.



We performed density functional theory (DFT) calculations for both *trans* and *cis* isomers of compound **10** in different oxidation states (neutral, radical cation, dication, and tetracation). The details of these studies for compounds **8** and **10** are given below in the “Theoretical Calculations” section. At this point we will mention the relevant results for *trans*-**10** and *cis*-**10** that shed light on the observed CV data (Figure 2). Calculations of the energies at both B3LYP/6-31G(d) and B3LYP/6-311G(2df,p)//B3LYP/6-31G(d) levels of theory gave qualitatively the same results. The theory predicts that in the neutral (**10**) and dication (**10**²⁺) states the *trans* isomers are more stable than the *cis*-isomers, although the difference in energy between the isomers is small (2.1–5.3 kJ mol⁻¹). In the radical cation state, *trans*-**10**^{•+} is considerably more stable (by 16.4–18.0 kJ mol⁻¹) than the *cis* isomer (Figure 3). The opposite situation was found for **10**⁴⁺, in which the *cis* isomer is more stable (by 24.7–25.3 kJ mol⁻¹) than the *trans* isomer (Figure 3).

In the light of these theoretical calculations, the observed CVs (Figures 1 and 2) can be rationalized as follows. In the neutral state compound **10** exists as the more stable *trans* isomer, and this configuration is retained when **10** is oxi-

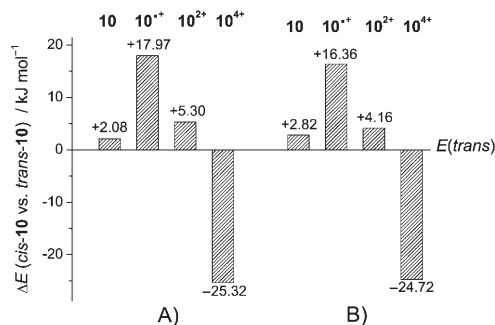


Figure 3. Calculated relative energies of *cis* versus *trans* isomers of compound **10** for the neutral, radical cation, dication and tetracation states at A) B3LYP/6-311G(2df,p)//B3LYP/6-31G(d) and B) B3LYP/6-31G(d)//B3LYP/6-31G(d) levels of theory. Unrestricted Hartree–Fock formalism was applied for the radical cations and restricted formalism was used for the neutral, dication, and tetracation states.

dized to $\mathbf{10}^+$ or $\mathbf{10}^{2+}$ (CV in Figure 1). However, oxidation to the tetracation results in isomerization into the more stable *cis*- $\mathbf{10}^{4+}$. Subsequent electrochemical reduction to the neutral state ($\mathbf{10}$) on the back scan proceeds differently at low and at high scan rates. At low scan rate of 30 mVs^{-1} , the reduction of *cis*- $\mathbf{10}^{4+}$ is accompanied by its isomerization from the *cis* to the more thermodynamically stable *trans* isomer, so the shape of the CV oxidation waves in the ($\mathbf{10}/\mathbf{10}^+/\mathbf{10}^{2+}$) region at further scans, as presented in Figure 2 a, is similar to that shown in Figure 1.

When the rate of the reverse scan is increased, the *cis*-*trans* isomerization is incomplete within the timescale of the CV experiment, and, therefore, a certain amount of compound $\mathbf{10}$ still exists in the *cis* configuration. This leads to the additional peaks (E_{pc} and E_{pa}) below the first oxidation potential $E_{1/2}^{\text{ox1}}$ (Figure 2b,c and Figures S3 and S4 in the Supporting Information), which we attribute to the reduction/oxidation processes for the *cis*- $\mathbf{10}^+/\mathbf{10}$ isomers.

To further support this interpretation, two additional CV experiments were performed at high scan rate (300 mVs^{-1}) starting from different potentials. On scanning from $+0.7 \text{ V}$ (*trans*- $\mathbf{10}^{2+}$ state) to negative potentials, the first voltammogram was “normal” in the ($\mathbf{10}/\mathbf{10}^+/\mathbf{10}^{2+}$) region, similar to that in Figure 1. On further scans, after oxidation of the species into *cis*- $\mathbf{10}^{4+}$, the CV became similar to that in Figure 2c, showing an additional peak for the *cis*- $\mathbf{10}/\text{cis-}\mathbf{10}^+$ isomers below the $E_{1/2}^{\text{ox1}}$ wave for the *trans*-isomer (Figure 4a). In contrast to these data, when the CV experiment was started at 1.4 V (*cis*- $\mathbf{10}^{4+}$ state), the first scan already demonstrated two closely-spaced $\mathbf{10}/\mathbf{10}^+$ redox processes from both *trans* and *cis* isomers. Similar CVs were obtained for the three subsequent cycles (Figure 4b).

In MeCN the CV similarly shows two consecutive reversible single-electron oxidation waves with $E_{1/2}^{\text{ox1}} = -0.118 \text{ V}$ and $E_{1/2}^{\text{ox2}} = +0.024 \text{ V}$ vs. Ag/Ag^+ , corresponding to the $\mathbf{10} \rightarrow \mathbf{10}^+ \rightarrow \mathbf{10}^{2+}$ transformations. Thus, changing the solvent from CH_2Cl_2 to MeCN results in a decrease in the difference between the first and the second oxidation potentials $\Delta E^{\text{ox2-ox1}}$ from 0.28 V to 0.14 V , that is, in a decrease of the thermodynamic stability of the $\mathbf{10}^+$ radical ion (characterized by disproportionation constant $K_{\text{dispr}} = [\text{D}][\text{D}^{2+}]/[\text{D}^+]^2$, D = donor, Table 1). These data agree with the solvent effects reported previously for other TTF vinyllogs substituted at the vinyl positions.^[10] On further oxidation in MeCN, compound $\mathbf{10}$ showed a third irreversible oxidation peak at $+0.84 \text{ V}$ (Table 1, Figure S7 in the Supporting Information).

Table 1. Redox potentials of compounds **8** and **10**.

Solvent	$E_{1/2}^{\text{ox1}}$ [V] ($\Delta E_{\text{pa-pc}}$ [mV])	$E_{1/2}^{\text{ox2}}$ [V] ($\Delta E_{\text{pa-pc}}$ [mV])	$E_{\text{pa}}^{\text{ox3}}$ [V]	$\Delta E^{\text{ox2-ox1}}$ [V]	K_{dispr} [M^{-1}] ^[c]
8 ^[a] MeCN	0.84 ^[d]				
10 ^[b] CH_2Cl_2	-0.003 (65)	+0.278 (62)	1.33	0.281	176×10^{-3}
10 ^[b] MeCN	-0.118 (64)	+0.024 (66)	0.84	0.142	5.84×10^{-3}

[a] Measured against Ag/AgCl reference electrode, scan rate 100 mVs^{-1} . [b] Measured against Ag/Ag^+ reference electrode, scan rate 100 mVs^{-1} . Fc/Fc^+ couple as an internal standard showed potentials $+0.130 \text{ V}$ (CH_2Cl_2) and $+0.079 \text{ V}$ (MeCN) against this electrode in our experiments. [c] Estimated by equation $\Delta E^{\text{ox2-ox1}} = E_{1/2}^{\text{ox2}} - E_{1/2}^{\text{ox1}} = -0.0591 \log K_{\text{dispr}}$. [d] Two electrons.

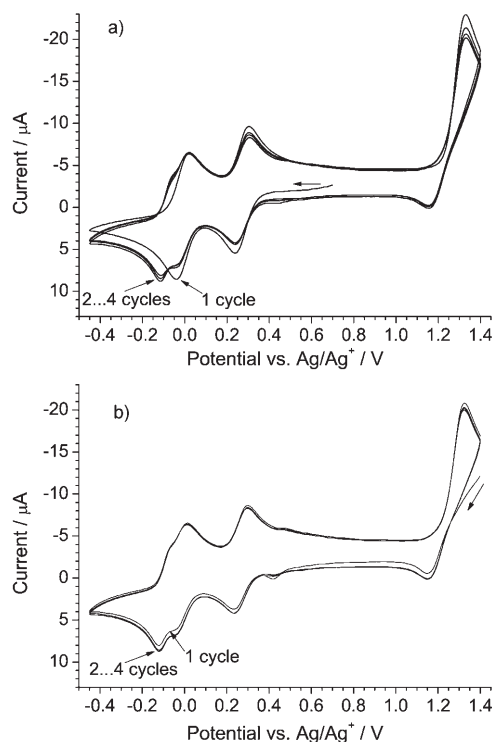


Figure 4. Cyclic voltammograms of compound **10** in CH_2Cl_2 , 0.2 M Bu_4NPF_6 ; four consecutive scans at scan rate of 300 mVs^{-1} : a) starting at $+0.70 \text{ V}$, scan to negative; b) starting at $+1.40 \text{ V}$, scan to negative.

Spectroelectrochemical studies: Spectroelectrochemical experiments (SEC) in CH_2Cl_2 and MeCN were performed to establish the spectroscopic signatures of the radical cation, dication, and tetracation species generated from compound **10**. In CH_2Cl_2 , compound **10** had two absorptions at $\lambda_{\text{max}} = 389$ and 410 nm with a shoulder at $\approx 450 \text{ nm}$. On oxidation, by applying a positive potential, these bands decreased, with the concomitant growth of low-energy absorptions of the $\mathbf{10}^+$ radical ion at $\lambda_{\text{max}} = 589, 703, \text{ and } 830 \text{ nm}$ (Figure 5a), with a clear isobestic point at 494 nm . Similar absorption features for other TTF vinyllogs have been reported in the literature.^[10]

An increase in the potential resulted in the disappearance of the absorption of $\mathbf{10}^+$ and the appearance of a new peak at $\lambda_{\text{max}} = 447 \text{ nm}$ with a low intensity broad band centered at 645 nm from $\mathbf{10}^{2+}$ (isobestic point at 523 nm ; Figure 5b). A further increase in the potential resulted in a blue shift in the absorption, which now peaked at 330 nm (Figure 5c). This hypsochromic shift observed in the range from 1.3 V to 1.6 V is entirely consistent with the $\mathbf{10}^{2+} \rightarrow \mathbf{10}^{4+}$ transformation, and the clean isobestic point (392 nm) leaves no room for the presence of the $\mathbf{10}^{3+}$ radical ion in the system. Such a species should display a bath-

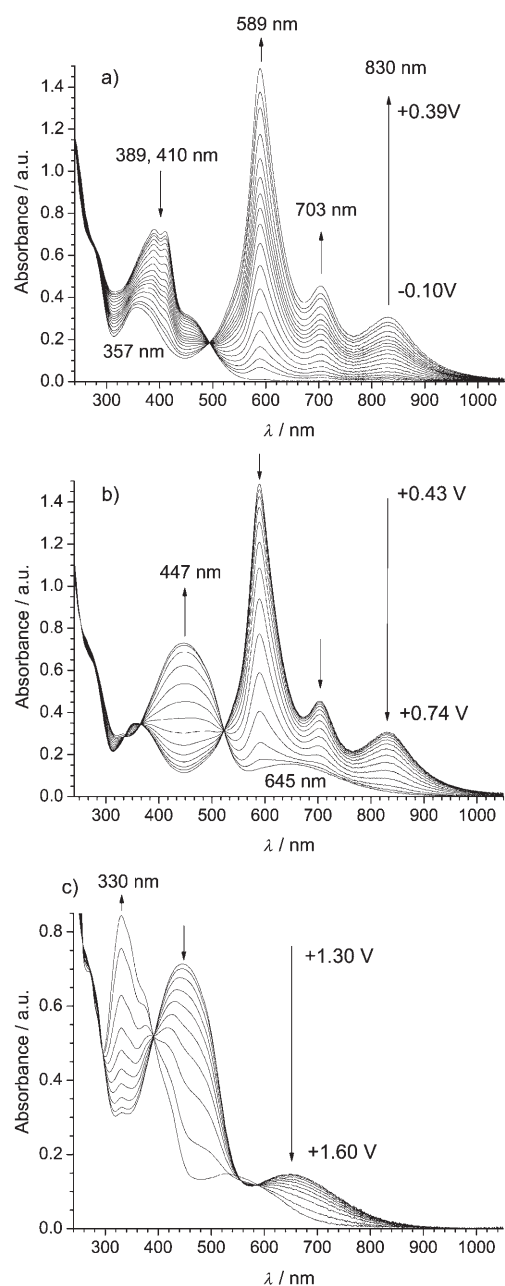


Figure 5. Spectroelectrochemistry of compound **10** in CH_2Cl_2 , 0.2 M Bu_4NPF_6 : a) $10^0 \rightarrow 10^+$, b) $10^+ \rightarrow 10^{2+}$, and c) $10^{2+} \rightarrow 10^{4+}$ (1 mm quartz cell, transmission mode, potentials are vs. Ag wire).

ochromic shift compared to 10^{2+} . The spectral evolutions during the electrochemical oxidation $10 \rightarrow 10^+ \rightarrow 10^{2+} \rightarrow 10^{4+}$ are represented in Figures 5 and 6.

Similar SEC experiments performed in MeCN demonstrated analogous spectral changes for the transformations $10 \rightarrow 10^+ \rightarrow 10^{2+}$, with absorption maxima for 10^+ and 10^{2+} at similar wavelengths to those in CH_2Cl_2 (Figures S8 and S9 in Supporting Information).

EPR studies: The electrochemical oxidation of **10** “in situ” in the EPR spectrometer cavity gave an intense, symmetri-

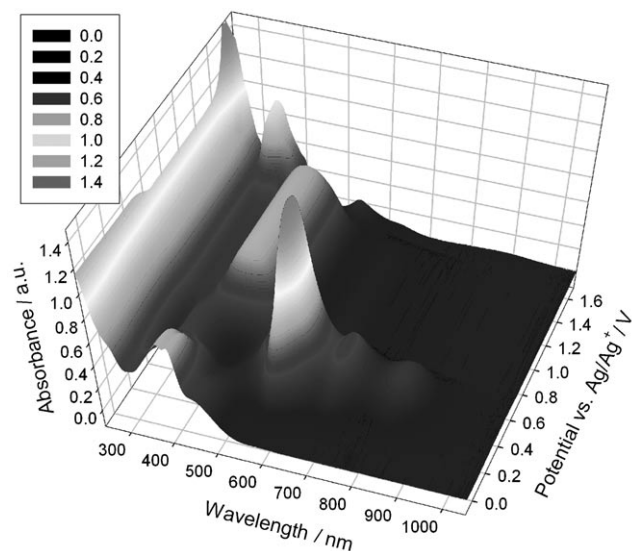


Figure 6. Three-dimensional representation of the SEC experiment for compound **10** in CH_2Cl_2 , 0.2 M Bu_4NPF_6 , 1 mm quartz cell, transmission mode; potentials are versus Ag wire.

cal EPR signal with fine structure and is assigned to 10^+ . The spectrum recorded at $E=0.4$ V (vs. Ag/AgCl) in a solution of 0.2 M Bu_4NPF_6 in CH_2Cl_2 is shown in Figure 7. On increasing the potential to $E=0.7$ V the signal disappeared due to the formation of 10^{2+} . This behavior is consistent with the CV and spectroelectrochemical studies presented above.

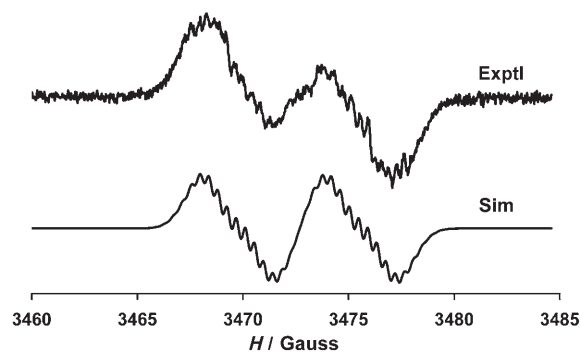


Figure 7. EPR spectrum of electrochemically generated 10^+ in $\text{CH}_2\text{Cl}_2/0.2$ M Bu_4NPF_6 solution (top) and its simulation (bottom).

Although it was not possible to simulate the EPR spectrum in optimal conditions because the signal did not show good resolution, the simulation (Figure 7) is good enough to establish that the spin distribution is delocalized over the whole molecule; that is, 10^+ should be viewed as a π -extended system. The hyperfine coupling constants obtained for the different protons from the best simulation are: $a(1\text{H})=5.8$ G, $a(1\text{H})=1.75$ G, $a(4\text{H})=0.32$ G, $a(4\text{H})=0.35$ G, and $a(12\text{H})=0.46$ G; g factor=2.00695 and line width=0.35 G. There are two protons with higher coupling

constants that can be ascribed to the ones on the bridge's double bonds. Most probably the one on the bridge of the vinylous TTF skeleton has the highest coupling, approaching 6 G, which is of similar order to the coupling shown by other vinylous TTF derivatives.^[4] The protons of the four methyl TTF substituents have the same coupling constant and those in the aromatic rings are divided in two sets of four equivalent protons with similar constants.

Radical cations derived from **11**, **12**, and **13** have been generated electrochemically following the same process, in a solution of 0.2 M Bu₄NPF₆ in CH₂Cl₂. The EPR spectra obtained in some cases were not symmetric, revealing the presence of more than one radical. In general, the pattern is a spectrum with two or more lines centered at $g = 2.0070$. Similarly to **10**, an increase in the potentials above that for generation of radical cation species resulted in disappearance of the EPR signals due to further oxidation to the EPR silent dication. The different shapes of the EPR spectra relative to that observed for **10**⁺ could be related to the facile oxidative dimerization of dithiafulvalenes to form TTF vinyl-ogs.^[11,24]

Charge-transfer complexation with 2,4,5,7-tetranitro-9-dicyanomethylene-fluorene: The strong electron donor **10** interacts with π -electron acceptors to form charge-transfer complexes (CTC) and radical-ion salts. Complexation of **10** with 2,4,5,7-tetranitrofluorene-9-dicyanomethylene-fluorene (DTeF) in polar solvents resulted in the appearance of three low energy absorption bands [λ_{max} 588, 703, 827 nm (in nitromethane, Figure 8a), 585, 701, 824 nm (in acetonitrile, Figure S10 in the Supporting Information)], characteristic for the **10**⁺ radical ion (see Figure 5a and Figures S5, S6, S8, and S9 in the Supporting Information). In addition to the absorption from **10**⁺ in these solutions, broad absorption bands in the NIR region were also observed: one band is at about $\lambda = 1000\text{--}1200$ nm (overlapping with an absorption of

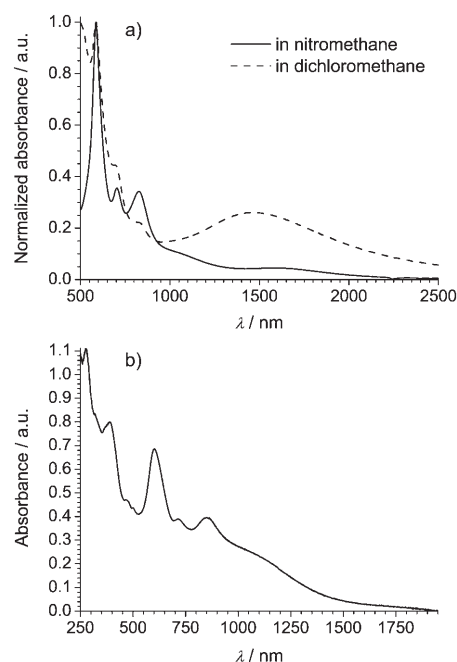
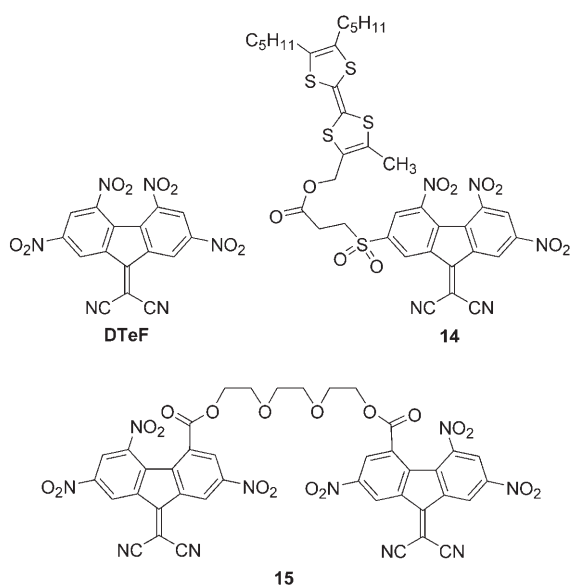


Figure 8. UV/Vis/NIR absorption spectra of the CTC between **10** and DTeF a) in nitromethane (solid line; $\lambda_{\text{max}} = 588, 703, 827, \sim 1000$ sh, 1590 nm) and dichloromethane (dashed line; $\lambda_{\text{max}} = 586, 694, 820$ sh, 1460 nm) and b) in the solid state (for CTC **10**-(DTeF)₂-2PhCl in KBr pellet (vs. KBr); $\lambda_{\text{max}} = 602, 713, 848, \sim 1000$ sh nm).

the **10**⁺ radical ion) and the second, less intense broad band is at $\lambda = 1300\text{--}2300$ nm (centered at ca. 1590 nm). Similar low-energy absorptions in the NIR region were previously observed for radical anions and CTCs of the fluorene acceptors. Thus, the CTC DTeF-TTF in CH₂Cl₂ showed a broad absorption band at 900–2000 nm, centered at about 1200 nm, and similar absorption in the NIR region was observed on electrochemical reduction of D-A (D = donor A = acceptor) dyad **14** to its radical ion state D-A^{•-} in SEC experiments ($\lambda_{\text{max}} = 1220$ nm).^[25] This indicates that complexation of donor **10** and acceptor DTeF results in a full electron transfer to form **10**⁺ and DTeF⁻ species in solution (and is probably the first example of full electron transfer for fluorene CTCs in solution). In the solid state it is known that fluorene acceptors and TTF-type donors form CTCs with different degrees of charge transfer (from neutral or partial charge transfer^[26,27] to full electron transfer in radical ion salts).^[21,28]

Studies of the solvent effect on charge transfer complexation between **10** and DTeF showed an appearance of three long-wavelength bands characteristic of the **10**⁺ radical ion in tetrahydrofuran, ethyl acetate, chloroform, and dichloromethane: see Figure 8a and Figures S10 and S11 in Supporting Information. On decreasing the solvent polarity, the intensity of the lowest energy NIR band increased significantly (relative to the bands of **10**⁺ at $\sim 600\text{--}800$ nm) with a blue shift from 1590 nm in nitromethane to 1460 nm in dichloromethane (Figure 8a).



The lowest energy absorption at ~1460–1590 nm could arise from the charge transfer in CTC $10^+\cdot\text{DTeF}^-$ or, possibly, from the mixed valence state between the neutral and radical anion states of the acceptor $\text{DTeF}^0\cdot\text{DTeF}^-$. We note for acceptor **15**, containing two nitrofluorene moieties connected by a flexible bridge, the electrochemical reduction in SEC experiments showed formation of a mixed valence state $\text{A}-\sigma\text{-A}^-$ (broad absorption at 1400–2500 nm with $\lambda_{\text{max}} = 1950$ nm, in DMF) proceeding to the diradical dianion state $\text{A}^--\sigma\text{-A}^-$ (800–1200 nm with $\lambda_{\text{max}} = 960$ nm).^[29]

In the solid state, CTC of **10** with DTeF grown from chlorobenzene showed the composition $10\cdot(\text{DTeF})_2\cdot 2\text{PhCl}$ by single-crystal X-ray analysis (see the next section). The absorption spectrum of this complex in KBr pellets again showed three bands characteristic for the 10^+ radical ion together with an intense broad absorption centered at ~1000–1100 nm (assigned to the fluorene anion radical) and a low intensity broad absorption at ~1500–1800 nm (Figure 8b). The solid-state IR spectrum of $10\cdot(\text{DTeF})_2\cdot 2\text{PhCl}$ (in KBr pellets) showed $\nu_{\text{C}\equiv\text{N}} = 2182.5\text{ cm}^{-1}$ (and a second weak signal at 2162 cm^{-1}). This value is significantly lower than that of neutral DTeF ($\nu_{\text{C}\equiv\text{N}} = 2233\text{ cm}^{-1}$ and a shoulder at 2226 cm^{-1}) (lit.^[21] $\nu_{\text{C}\equiv\text{N}} = 2233\text{ cm}^{-1}$) and similar to that of the radical anion salt $\text{Li}^+\cdot\text{DTeF}^-$ (2185 cm^{-1}).^[25] These data point to a radical ion structure $10^+\cdot(\text{DTeF})_2\cdot 2\text{PhCl}$.

X-ray crystallographic studies of **8** and $10\cdot(\text{DTeF})_2\cdot 2\text{PhCl}$:

In the X-ray crystal structure of **8** (Figure 9) the dithiolebutadiene moiety is disordered between two orientations with occupancies 88.4(1)% and 11.6(1)%, which differ in the configuration around the $\text{C7}=\text{C8}$ bond and can be (roughly) described as related by the mirror plane of the thioxanthene moiety. The thioxanthene unit is folded with the benzene rings forming an interplanar angle of 143.0° . The butadiene moiety is slightly distorted from planarity by twists of 4.4 , 3.1 , and 8.0° around the $\text{C1}=\text{C6}$, $\text{C6}-\text{C7}$, and $\text{C7}=\text{C8}$ bonds, respectively.

We could not grow single crystals of neutral compound **10** suitable for X-ray analysis. The crystals of the CTC obtained by co-crystallization of **10** and acceptor DTeF in chlorobenzene were exceedingly small and twinned. Thus the quality of X-ray diffraction data was rather poor, but sufficient to provide clear evidence of the stoichiometry of the complex as $10\cdot(\text{DTeF})_2\cdot 2\text{PhCl}$ and the general conformation and packing motif, although not of the accurate bond lengths. The asymmetric unit comprises one formula unit. Both SEC experiments and CTC between **10** and DTeF in solutions

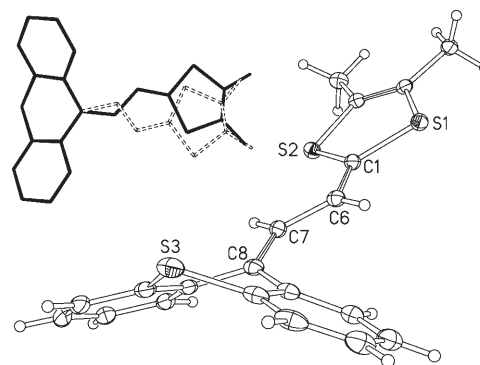


Figure 9. X-ray molecular structure of **8** (thermal ellipsoids at the 50% probability level) and the mode of disorder (insert).

(vide supra) establish the radical cation nature for the donor (10^+) in the crystal and hence the $10^+\cdot(\text{DTeF})_2\cdot 2\text{PhCl}$ formulation of the complex. The radical cation is nonplanar due to steric overcrowding (Figure 10a), which indeed is unavoidable in any of its oxidation states, 10 , 10^+ , or 10^{2+} (see calculations below). The thioxanthene system (**B**) is folded along the $\text{S3}\cdots\text{C10}$ vector, its benzene rings form a dihedral angle of 143° , and the S5 atom is disordered. The angle between two planar 1,3-dithiol-2-ylidene moieties (**A** and **C**) is 64° , that between moiety **A** and the $\text{C5}-\text{C9}-\text{C10}-\text{C11}-\text{C17}$ plane is 73° (Figure 10a).

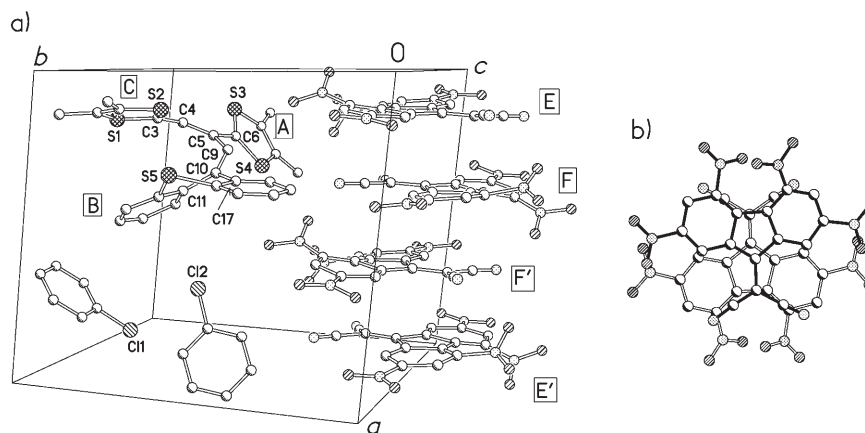


Figure 10. a) Fragment of the crystal structure of $10\cdot(\text{DTeF})_2\cdot 2\text{PhCl}$, showing one asymmetric unit and inversion equivalents of molecules **E** and **F** (primed). Disorder is not shown. b) Overlap of DTeF molecules, viewed down the *a* axis.

Two symmetrically independent DTeF moieties, **E** and **F**, have a 1– charge and one unpaired electron between them. The low precision of the data does not establish whether DTeF^- and DTeF^0 occupy specific sites or are randomly distributed. Both moieties adopt similar, somewhat warped, conformations, typical for DTeF itself^[30] and all its derivatives, due to steric repulsion between the nitro groups in 4- and 5-positions. However, warping does not prevent the DTeF units from assembling into an infinite stack, in a $\cdots\text{E}-\text{F}-\text{F}-\text{E}-\text{E}-\text{F}-\text{F}\cdots$ succession (Figure 10a). The fluorene

mean planes of the two independent units (and hence of all DTfE units in the triclinic crystal structure) are parallel within experimental error and normal to the direction of the stack (crystal axis x). Within a stack, the adjacent units **E** and **F** are related by a local (noncrystallographic) inversion center ($1/4 0 1/2$), whereas the pairs **EE** and **FF** are related by crystallographic inversion centers ($00 1/2$) and ($1/2 0 1/2$), respectively, or their equivalents. Thus each contact in the stack is of a head-to-tail kind, with the exocyclic C=C bond of one molecule perfectly overlapped by the five-membered ring of the other molecule (Figure 10b). The mean interplanar separation **E–F** of 3.05 Å is characteristic for “long-bonded π dimers”, which are often formed by spontaneous self-association of various organic radicals, and are stable both in solution and in the solid state.^[31] Along a stack, such separations alternate with longer **E–E** and **F–F** separations of approximately 3.3 Å, which are still shorter than “normal” van der Waals contacts of 3.4–3.5 Å.

It is known that nitrosubstituted fluorene acceptors readily form CTCs with electron donors,^[26,32] including numerous TTF-family donors.^[21d,25,27,28] X-ray structures are known for many of these CTCs of different stoichiometries,^[25,27] but in all cases the fluorene acceptors form alternating stacks with the donor molecules [DADA (1:1), DAADAA (1:2) or DADAA (2:3) motifs] typical for semiconductive CTCs. The only exception is a three-component (1:1:1) CTC of 3,3'-diethylthiazolinocarbocyanine with TCNQ and 9-dicyanomethylene-2,4,7-trinitrofluorenone (DTF).^[33] This structure contains a mixed stack of two different acceptors, presumably TCNQ^- ions and DTF molecules alternating [$A^1A^2A^1A^2$] with nearly uniform interplanar separations of about 3.3 Å. To the best of our knowledge, **10**·(DTfE)₂·2PhCl is the first definitive example of a CTC with stacks consisting only of a fluorene acceptor.^[34] Such arrangement may be facilitated by the awkward conformation of the **10**^{•+} radical ion, which precludes effective stacking (π - π overlap) with a planar moiety. Thus **10**^{•+} and two independent PhCl molecules (one of them disordered) occupy channels between the acceptor columns (additional packing diagrams are shown in Figure S22 in the Supporting Information).

Theoretical calculations: We performed quantum chemical calculations of the geometries and electronic structures of compounds **8** and **10** in different oxidation states (neutral, radical cation, dication, and tetracation) by DFT methods. The geometries of **8**, **8**^{•+}, **8**²⁺, **10**, **10**^{•+}, **10**²⁺, and **10**⁴⁺ were optimized at the B3LYP/6-31G(d) level of theory, and the electronic structures were calculated at the B3LYP/6-311G-(2df,p) level for B3LYP/6-31G(d) optimized geometries (Figures S12–S21 and Tables S1–S11 in the Supporting Information).

The geometry of the thioxanthene fragment provides a good indication of the charge on this moiety: it has a strongly folded conformation when neutral, whereas it is planar when positively charged.^[35] In the neutral state of molecule **8** the thioxanthene moiety adopts a nonplanar saddle-shape

and the butadiene chain is only slightly twisted around the central =CH–CH= bond (Figure 11a), which is similar to the conformation in the X-ray structure (Figure 9). Only minor

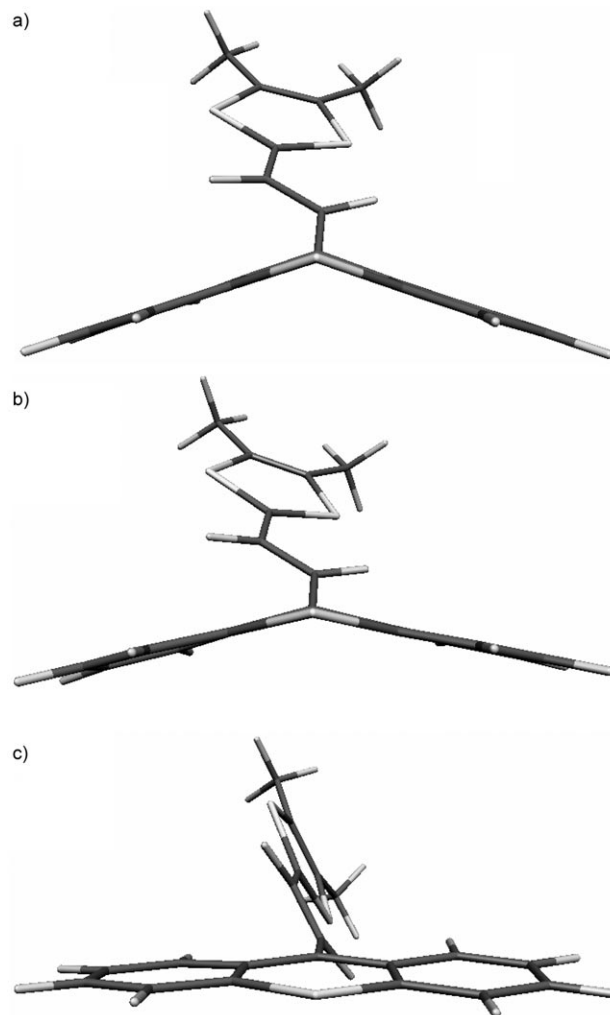
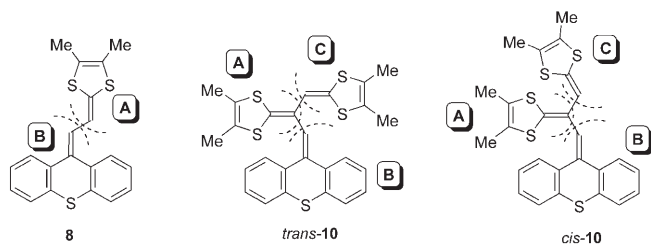


Figure 11. B3LYP/6-31G(d) optimized geometries of a) **8**, b) **8**^{•+}, and c) **8**²⁺.

conformational changes accompany its oxidation to **8**^{•+} (Figure 11b; some planarization of the thioxanthene moiety) and the charge and the spin density are nearly symmetrically distributed between the dithiole and thioxanthene moieties (Table 2). On the other hand, in the dication state **8**²⁺ the thioxanthene moiety is fully planarized and both the dithiolium ring and the butadiene bridge are twisted with respect to the thioxanthene plane, with a dihedral angle of ~65° (Figure 11c). Mulliken charge population analysis of the dication state reveals that both the dithiole and thioxanthene moieties have almost equal positive charges (+0.98 and +1.02, respectively; Table 2), with negligibly small charge on the central =CH–CH= bridge (–0.04).

The HOMO in **8** is delocalized between the dithiole moiety and the butadiene chain forming bonding orbitals on the double C=C bonds of the butadiene bridge. These orbi-

Table 2. Charge distribution between the dithiole and thioxanthene moieties^[a] in radical cation, dication, and tetracation states of compounds **8** and **10** according to B3LYP/6-311G(2df,p)//B3LYP/6-31G(d) calculations.



	A	B	C
8 ^{•+}	+0.50	+0.50	–
8 ²⁺	+0.98	+1.02	–
<i>trans-10</i> ^{•+}	+0.45	+0.11	+0.44
<i>trans-10</i> ²⁺	+0.84	+0.58	+0.58
<i>trans-10</i> ⁴⁺	+1.07	+1.71	+1.22
<i>cis-10</i> ^{•+}	+0.45	+0.29	+0.26
<i>cis-10</i> ²⁺	+0.85	+0.81	+0.34
<i>cis-10</i> ⁴⁺	+0.89	+1.69	+1.42

[a] The sums of Mulliken atom charges on the fragments **A**, **B**, and **C** are given.

tals are antibonding in the LUMO, whereas the LUMO in total is substantially shifted onto the thioxanthene moiety (Figure 12).

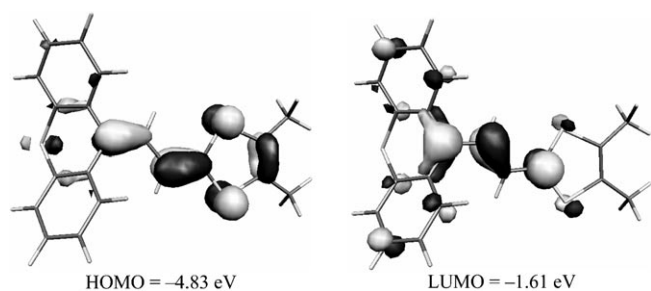


Figure 12. B3LYP/6-311G(2df,p)//B3LYP/6-31G(d) frontier orbitals for the neutral state of compound **8**.

In the optimized geometries of both *trans*- and *cis*-**10** isomers, in the neutral states the thioxanthene moiety adopts a nonplanar saddle-shaped conformation, similar to **8** (Figures 13a and 14a). The steric effect of the bulky thioxanthene moiety forces the vinylogous TTF fragment in *trans*-**10** to be nonplanar, with folding along the central C–C bond of the butadiene bridge by ~40° with additional distortion of the dithiole moieties, the planes of which form a dihedral angle of ~30°. Nonplanarity of the vinylogous TTF fragment in *cis*-**10** is evidently due to steric repulsion between the dithiole moieties.

The thioxanthene moiety retains its saddle-shaped conformation in both the *trans* and *cis* isomers of the **10**^{•+} radical ion, although there is a tendency for planarization, which is more pronounced for *cis*-**10**^{•+} than *trans*-**10**^{•+} (Figures 13b and 14b). The difference in positive charge localization on the thioxanthene moieties in *cis*- and *trans*-**10**^{•+} (+0.29 and +0.11, respectively, Table 2) reflects these features. In *trans*-

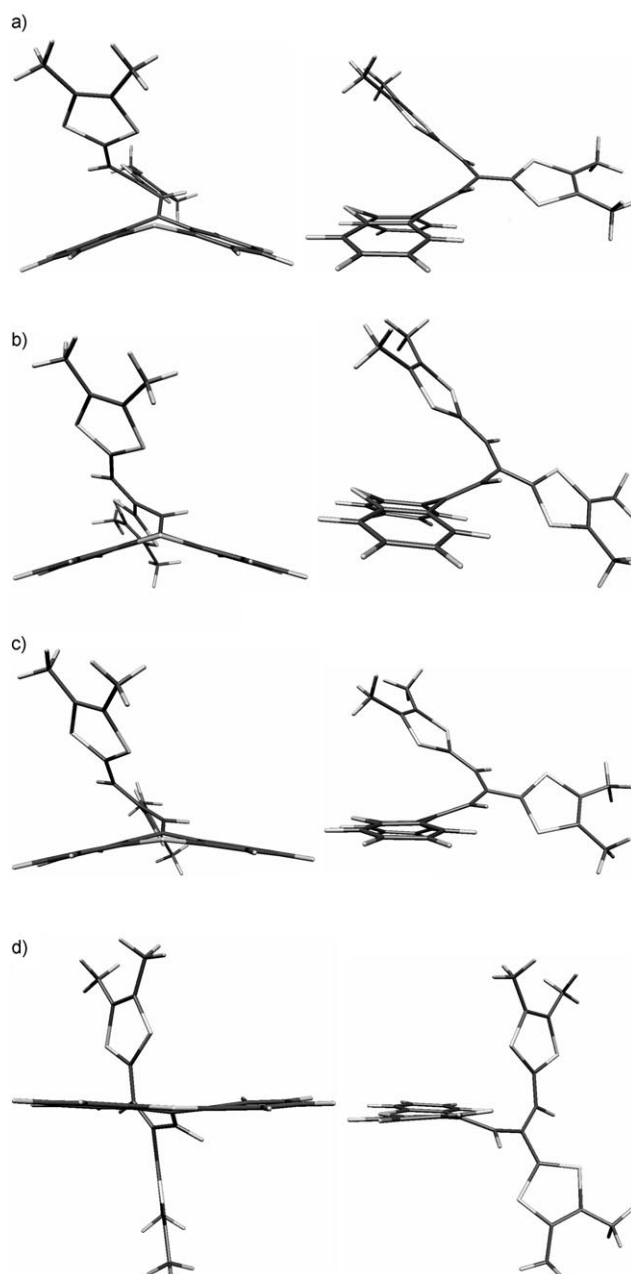


Figure 13. B3LYP/6-31G(d) optimized geometries of a) *trans*-**10**, b) *trans*-**10**^{•+}, c) *trans*-**10**²⁺, and d) *trans*-**10**⁴⁺.

10^{•+} the positive charge and spin density are predominantly delocalized on the vinylogous TTF moiety (**A**+**C**, Table 2).

For *trans*-**10**²⁺ the thioxanthene moiety becomes more planar than in the neutral or radical cation states, although its folded conformation still remains to a certain extent, whereas for *cis*-**10**²⁺ it is almost planar (Figures 13c and 14c). These geometrical differences between the isomers are in good agreement with the differences in their charge distribution: the positive charge on the thioxanthene moiety is greater for *cis*-**10**²⁺ (+0.81) than for *trans*-**10**²⁺ (+0.58) (**B**, Table 2).

In **10**⁴⁺, the thioxanthene moiety is planar for both *cis* and *trans* isomers (Figures 13d and 14d), carrying positive

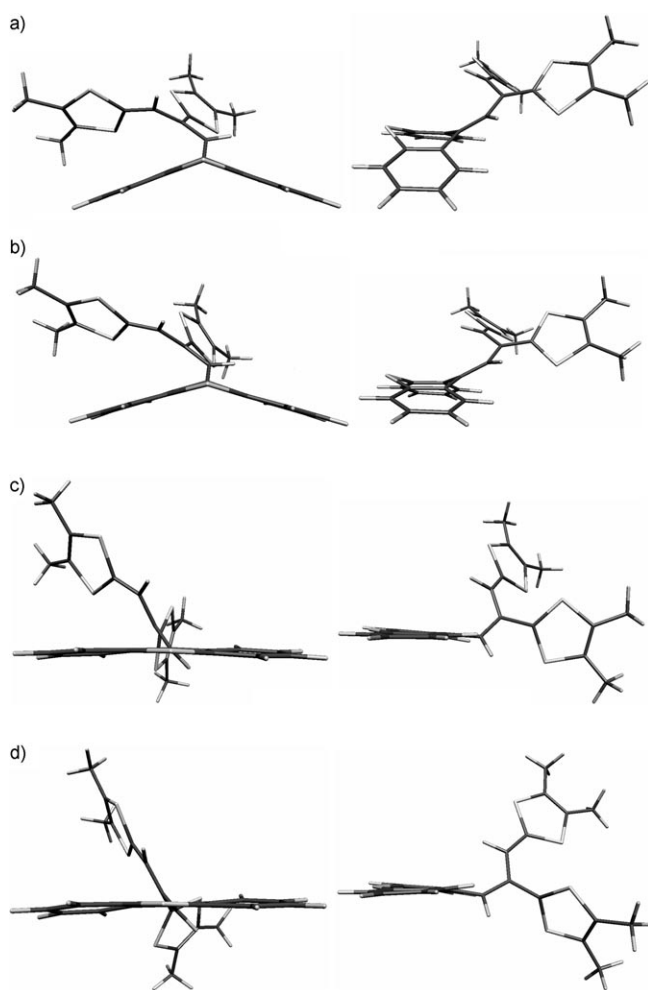


Figure 14. B3LYP/6-31G(d) optimized geometries of a) *cis-10*, b) *cis-10*⁺, c) *cis-10*²⁺, and d) *cis-10*⁴⁺.

charges of +1.56 and +1.59, respectively (+1.69 and +1.71 for moieties **B**, Table 2). The central =CH–C(=)–CH= exocyclic bridge between the redox-active dithiole and thioxanthene units is only partly charged for both *cis*- and *trans-10*⁴⁺ ions (+0.19 and +0.11, respectively). For *trans-10*⁴⁺, relative to its lower oxidation states, the orientation of the vinyllogous TTF moiety is substantially changed, becoming nearly orthogonal to the thioxanthene moiety (Figure 13). There are no such drastic changes in the relative orientations of these moieties for *cis-10* depending on the oxidation state (Figure 14).

The calculated bond lengths in the central exocyclic fragments of compounds **8** (*a*, *b*, *c*) and **10** (*a*, *b*, *c*, *d*, *e*) at different oxidation states are collated in Table 3. For neutral molecule **8** there is good agreement between the calculated values and the X-ray diffraction experiment: bonds *a* and *c* are essentially double C=C bonds with the length of *b* (1.438 Å) close to the standard 1.455(11) Å for a single C(sp²)–C(sp²) bond in a planar (conjugated) butadiene system^[36] (Table 3). On oxidation to **8**⁺, all three bonds almost equalize indicating pronounced π delocalization along the bridge, whereas further oxidation to **8**²⁺ results in

Table 3. B3LYP/6-31G(d) calculated bond lengths [*a–e* in Å] in the central butadiene fragment of compounds **8** and **10** at different oxidation states.

	<i>a</i>	<i>b</i>	<i>c</i>	<i>d</i>	<i>e</i>
8	1.360	1.438	1.367	–	–
8 ⁺	1.358(2) ^[a]	1.439(3) ^[a]	1.359(2) ^[a]	–	–
8 ²⁺	1.398	1.399	1.406	–	–
8 ²⁺	1.450	1.353	1.485	–	–
<i>trans-10</i>	1.370	1.470	1.363	1.467	1.354
<i>trans-10</i> ⁺	1.409	1.478	1.365	1.415	1.391
<i>trans-10</i> ²⁺	1.465	1.431	1.408	1.414	1.401
<i>trans-10</i> ⁴⁺	1.481	1.448	1.422	1.411	1.419
<i>cis-10</i>	1.376	1.464	1.363	1.467	1.354
<i>cis-10</i> ⁺	1.419	1.447	1.382	1.437	1.380
<i>cis-10</i> ²⁺	1.475	1.386	1.464	1.439	1.385
<i>cis-10</i> ⁴⁺	1.502	1.410	1.461	1.419	1.408

[a] Experimental (X-ray crystal structure, major conformer).

the bridge –CH=CH– unit with an essentially double central bond (*b* = 1.353 Å).

Nonplanarity of the vinyllogous TTF moiety in **10** arising from steric hindrance, as discussed above, diminishes the conjugation between the dithiole moieties and their conjugation with the thioxanthene moiety. As a result, the length of the bond *b* is increased from 1.438 Å in **8** to 1.464–1.470 Å in **10**, which is similar to the length of bond *d* (1.467 Å) between the dithiole units (Table 3). The same steric influence of the bulky thioxanthene moiety hinders the shortening of bond *b* to the normal double C=C bond length, which is somewhat longer than that in **8**²⁺ (*b* = 1.353, 1.431, and 1.378 Å for **8**²⁺, *trans-10*²⁺, and *cis-10*²⁺, respectively). The precision of the X-ray experiment is insufficient for meaningful comparison.

Conclusions

We have used Horner–Wadsworth–Emmons reactions of (1,3-dithiol-2-yl)phosphonate reagents to prepare novel vinyllogous π -electron donors, notably the sterically crowded cross-conjugated derivative 9-[2,3-bis-(4,5-dimethyl-1,3-dithiol-2-ylidene)-propylidene]thioxanthene (**10**). Detailed electrochemical and spectroscopic properties, X-ray analysis, and DFT calculations are reported. Compound **10** displays multistage redox behavior in solution with a fascinating and subtle interplay of electronic and structural properties at the different redox states. The overall electrochemical process can be represented by **10** → **10**⁺ → **10**²⁺ → **10**⁴⁺ with good reversibility for the **10** → **10**⁺ → **10**²⁺ transformations. The tetracation stage is characterized by aromaticity of the dithiolium and thioxanthenium rings. An unexpected feature is that

at fast scan rates both *trans* and *cis* isomers of **10** and **10⁺** were observed during the reduction of **10⁴⁺** [*trans* and *cis* refer to the arrangement of the two dithiole moieties with respect to the central =C(R)–C(H)= fragment] due to incomplete isomerization of the *cis* structure within the time-scale of the experiment. A very twisted structure of **10⁺** has been observed in the X-ray crystal structure of the charge-transfer complex **10⁺**·(DTeF)₂[–]·2 PhCl (DTeF = 2,4,5,7-tetranitrofluorene-9-dicyanomethylenefluorene). For future work the synthetic methodology should be adaptable to related vinylogous and cross-conjugated π systems, which will be designed to probe further the fundamental structural and electronic properties of these fascinating compounds.

Experimental Section

Thioxanthen-9-ylideneacetaldehyde (5): Phosphorus oxychloride (5.8 mL, 62.17 mmol) was added slowly to DMF (20 mL) cooled to 0°C in an ice bath. A solution of **4**^[18] (2.176 g, 10.36 mmol) in DMF (30 mL) was slowly added to this mixture. The mixture was warmed to room temperature and was maintained at 60°C overnight, then poured into iced water and neutralized to pH 7 with 10% sodium hydroxide solution. The solution was extracted with chloroform, and the organic phase was dried over MgSO₄ and evaporated. The residue was subjected to chromatography on silica (eluent CH₂Cl₂/hexane, 4:1 v/v) to afford compound **5** (1.44 g, 58%), a yellow solid. M.p. 108–110°C; ¹H NMR (300 MHz, CDCl₃): δ = 9.83 (d, *J* = 7.8 Hz, 1H; CHO), 7.68 (m, 1H), 7.56 (dd, *J* = 7.5, 1.2 Hz, 2H), 7.50 (m, 1H), 7.47–7.32 (m, 4H), 6.42 ppm (d, *J* = 7.8 Hz, 1H); ¹³C NMR (75 MHz, CDCl₃): δ = 193.29, 152.65, 134.12, 134.02, 132.14, 131.64, 129.83, 129.61, 129.35, 127.72, 127.66, 126.68, 126.52, 126.24, 126.21 ppm. MS (CI+): *m/z* (%): 239 (100) [*M*]⁺; UV/Vis (CHCl₃): λ_{max} = 386 nm; elemental analysis calcd (%) for C₁₅H₁₀OS (238.05): C 75.60, H 4.23; found: C 75.46, H 4.30.

9-[2-(4,5-Dimethyl-1,3-dithiol-2-ylidene)ethylidene]thioxanthene (8): *n*-Butyllithium (1.6 M in hexanes, 6 mL, 9.6 mmol) was added to a stirred solution of reagent **6** (2.12 g, 8.72 mmol), in dry THF (75 mL) at –78°C, and the mixture was stirred for 30 min. Compound **5** (2.07 g, 8.72 mmol) dissolved in THF (75 mL) was added slowly and the mixture was left to warm to room temperature overnight. Solvents were removed in vacuo and the residue was purified by chromatography on silica gel (eluent CH₂Cl₂), and then on alumina (eluent CH₂Cl₂/hexane, 1:1 v/v) to afford compound **8** (2.0 g, 65%) as red crystals. M.p. 193–195°C. ¹H NMR (400 MHz, CDCl₃): δ = 7.52 (dd, 1H; *J* = 8.0 MHz, 1.2 MHz), 7.50 (dd, *J* = 8.0, 1.2 Hz, 1H), 7.40 (m, 1H), 7.34 (m, 1H), 7.28–7.24 (m, 2H), 7.22–7.15 (m, 2H), 6.52 (d, *J* = 11.8 Hz, 1H), 6.34 (d, *J* = 11.8 Hz, 1H), 1.97 (s, 3H; CH₃), 1.93 ppm (s, 3H; CH₃); ¹³C NMR (100 MHz, CDCl₃): δ = 140.23, 138.64, 134.32, 133.74, 131.96, 130.07, 129.46, 127.24, 127.07, 126.99, 126.93, 126.65, 126.32, 126.09, 125.35, 122.21, 121.95, 109.12, 13.92, 13.57 ppm; MS (EI): *m/z* (%): 352 (100) [*M*]⁺; UV/Vis (CHCl₃): λ_{max} = 423 nm; elemental analysis calcd (%) for C₂₀H₁₆S₃ (352.04): C 68.14, H 4.57; found: C 67.86, H 4.57.

2-(4,5-Dimethyl-1,3-dithiol-2-ylidene)-3-thioxanthen-9-ylidenepropionaldehyde (9): Phosphorus oxychloride (1.74 mL, 18.75 mmol) was added slowly to DMF (10 mL) cooled in an ice bath at 0°C. A solution of compound **8** (1.1 g, 3.12 mmol) in DMF (15 mL) was slowly added to this mixture. The mixture was warmed to room temperature and was maintained at 60°C overnight. The reaction mixture was poured into iced water and neutralized to pH 7 with 10% sodium hydroxide solution. The solution was extracted with chloroform, and the organic phase was dried over MgSO₄ and evaporated. The residue was subjected to chromatography on silica (eluent, dichloromethane/hexane 1:1 v/v). After evaporation, acetone was added and the resulting crude solid was filtered and washed with acetone to give compound **9** (1.13 g, 95%) as yellow crystals. M.p. 242–244°C; ¹H NMR (500 MHz, CDCl₃): δ = 8.88 (s, 1H; CHO),

7.73 (d, *J* = 8.0 Hz, 1H), 7.44 (d, *J* = 8.0 Hz, 2H), 7.37 (d, *J* = 8.0 Hz, 1H), 7.34 (dd, *J* = 7.5, 7.5 Hz, 1H), 7.27 (dd, *J* = 7.5, 7.5 Hz, 1H), 7.19 (dd, *J* = 7.5, 7.5 Hz, 1H), 7.13 (dd, *J* = 7.5, 7.5 Hz, 1H) 6.53 (s, 1H; CH), 2.26 (s, 3H; CH₃), 2.21 ppm (s, 3H; CH₃); ¹³C NMR (125 MHz, CDCl₃): δ = 183.78, 137.25, 136.07, 135.35, 134.28, 133.72, 132.70, 130.07, 128.78, 127.94, 127.42, 127.30, 127.23, 126.96, 126.45, 125.47, 124.34, 123.37, 116.86, 13.74, 13.41 ppm; IR (KBr): ν̄ = 2900, 1684, 1653, 1627, 1458, 1419, 1380, 1259, 858, 762, 739, 621, 543 cm^{–1}; MS (EI): *m/z* (%): 380 (89) [*M*]⁺, 155 (100) [*M*–225]⁺; UV/Vis (CHCl₃): λ_{max} = 429 nm; elemental analysis calcd (%) for C₂₁H₁₆OS₃ (380.04): C 66.28, H 4.24; found: C 66.25, H 4.14.

9-[2,3-Bis-(4,5-dimethyl-1,3-dithiol-2-ylidene)propylidene]thioxanthene (10): Following the procedure described for **8**, compound **6** (0.319 g, 1.31 mmol), *n*BuLi (0.9 mL, 1.44 mmol), and compound **9** (0.50 g, 1.31 mmol) were reacted. After evaporation and chromatography on silica (eluent, dichloromethane), recrystallization from hexane gave compound **10** (0.15 g, 23%) as a red powder. M.p. 201–203°C; ¹H NMR (300 MHz, C₆D₆): δ = 7.95–7.87 (m, 2H), 7.33–7.26 (m, 2H), 7.07–6.93 (m, 2H), 6.93–6.83 (m, 2H), 6.70 (s, 1H; –CH=), 6.24 (s, 1H; –CH=), 1.37 (s, 3H; CH₃), 1.333 (s, 3H; CH₃), 1.324 (s, 3H; CH₃), 1.30 ppm (s, 3H; CH₃); ¹³C NMR (75 MHz, C₆D₆): δ = 137.96, 137.40, 134.26, 133.70, 133.25, 132.87, 129.29, 128.21, 127.89, 127.59, 127.13, 127.11, 126.88, 126.44, 126.04, 125.79, 124.82, 123.53, 122.54, 120.40, 118.58, 110.54, 13.21, 13.02, 12.99, 12.59 ppm. MS (EI): *m/z* (%): 494 (100) [*M*]⁺; MS (CI+): *m/z* (%): 495 (100) [*M*+H]⁺; UV/Vis (CHCl₃): λ_{max} = 389, 410 nm; elemental analysis calcd (%) for C₂₆H₂₂S₅ (494.03): C 63.11, H 4.48; found C 63.07, H 4.60.

Complex **10**·(DTeF)₂·2PhCl was obtained by mixing hot solutions of donor **10** and acceptor DTeF in chlorobenzene and storing the resulting solution of the CTC at room temperature.

9-[2-(4-Methyl-1,3-dithiol-2-ylidene)ethylidene]thioxanthene (11): By analogy with the preparation of **8**, compound **7** (0.80 g, 3.48 mmol), *n*BuLi (2.4 mL, 3.83 mmol), and compound **5** (0.83 g, 3.48 mmol) were stirred overnight. After evaporation and chromatography on silica (eluent, dichloromethane), and then on alumina (eluent CH₂Cl₂/hexane, 1:1 v/v), compound **11** was obtained (0.657 g, 56%) as yellow powder. M.p. 163–165°C; ¹H NMR (200 MHz, CDCl₃): δ = 7.53 (m, 2H), 7.41 (m, 2H), 7.35–7.13 (m, 4H), 6.62 (2d, *J* = 11.8 Hz, 1H; CH=CH, two isomers), 6.35 (d, *J* = 11.8 Hz, 1H; CH=CH), 5.85 (s, 1H; H-dithiole), 2.08 2.05 ppm (2s; CH₃, two isomers); ¹³C NMR (100 MHz, CDCl₃): δ = 140.23, 138.64, 134.32, 133.74, 131.96, 130.08, 129.46, 127.24, 127.07, 126.99, 126.92, 126.65, 126.32, 126.09, 125.35, 122.21, 121.95, 109.12, 13.91, 13.96 ppm; CH₃, two isomers); MS (EI+): *m/z* (%): 338 (100) [*M*]⁺; UV/Vis (CHCl₃): λ_{max} = 391 nm; elemental analysis calcd (%) for C₁₉H₁₄S₃ (338.03): C 67.41, H 4.17; found: C 67.26, H 4.45.

5-Methyl-2-(2-thioxanthen-9-ylideneethylidene)-1,3-dithiole-4-carboxylic acid methyl ester (12): *n*-Butyllithium (1.6 M in hexane, 3.77 mL, 6.03 mmol) was added to a stirred solution of compound **11** (1.85 g, 5.48 mmol) in dry THF (1000 mL) under N₂ at –78°C. The reaction mixture was stirred for 2 h. Methyl chloroformate (0.43 mL, 5.48 mmol) was added and the mixture was stirred and left to warm to room temperature overnight. The solvents were removed in vacuo and the residue was purified by chromatography on silica (eluent, dichloromethane/hexane; initially 3:1 v/v, then 1:1 v/v) to afford compound **12** (1.74 g, 80%) as yellow crystals. M.p. 97–99°C; ¹H NMR (300 MHz, CDCl₃): δ = (7.52 (2dd, *J* = 7.8, 7.8 Hz, 1H; two isomers), 7.47 (2d, *J* = 7.5 Hz, 1H; two isomers), 7.42 (m, 1H), 7.35 (m, 1H), 7.31–7.17 (m, 4H), 6.54, 6.48 (2d, *J* = 11.7 Hz, 1H; CH=CH, two isomers), 6.31, 6.25 (2d, *J* = 11.7 Hz, 1H; CH=CH, two isomers), 3.81, 3.78 (2s, 3H; CH₃, two isomers), 2.42, 2.38 ppm (2s, 3H; CH₃, two isomers); ¹³C NMR (125 MHz, CDCl₃): δ = 138.12, 136.22, 133.86, 133.84, 131.99, 131.95, 129.49, 129.46, 127.39, 127.37, 127.33, 127.30, 126.99, 126.96, 126.40, 126.35, 126.16, 126.11, 126.07, 126.01, 125.50, 125.37, 125.33, 110.85, 110.76, 52.73, 52.61; CO₂CH₃, two isomers), 16.32, 15.99 ppm; CH₃, two isomers);^[37] MS (EI): *m/z* (%): 396 (100) [*M*]⁺; UV/Vis (CHCl₃): λ_{max} = 406 nm; C₂₁H₁₆O₂S₃ (396.03): C 63.61, H 4.07; found: C 63.38, H 4.03.

[5-Methyl-2-(2-thioxanthen-9-ylideneethylidene)-1,3-dithiol-4-yl]methanol (13): Lithium aluminium hydride (0.688 g, 18.14 mmol) was added to

a stirred solution of compound **12** (1.80 g, 4.53 mmol) in dry THF (100 mL) under N₂ at -78 °C, and the resultant mixture was stirred for 2 h at 20 °C. After the addition of dropwise sodium sulphate decahydrate (in excess; to destroy unreacted LiAlH₄), the mixture was stirred for 30 min, then filtered through Celite while washing with methanol. Evaporation of the filtrate gave compound **13** (1.17 g, 70%) as yellow crystals. M.p. 88–90 °C; ¹H NMR (200 MHz, CDCl₃): δ = 7.58–7.49 (m, 2H), 7.47–7.41 (m, 1H), 7.40–7.15 (m, 5H), 6.58, 6.57 (2d, *J* = 11.6 Hz, 1H; CH=CH, two isomers), 6.37, 6.33 (2d, *J* = 11.6 Hz, 1H; CH=CH, two isomers), 4.40, 4.37 (2s, 2H; CH₂, two isomers), 2.07, 2.03 ppm (2s, 3H; CH₃, two isomers); ¹³C NMR (100 MHz, [D₆]DMSO): δ = (141.81, 141.75), 138.24, 133.74, 133.03, (131.33, 131.30), 130.74, 130.15, 129.75, (129.54, 129.37), (128.28, 128.27), 128.07, 127.62, (127.45, 127.36), (127.08, 127.04), 126.51, (125.77, 125.73), 124.17, 123.46, (108.77, 108.70), (57.10, 56.93; CH₂ two isomers), (14.04, 13.72 ppm; CH₃, two isomers);³⁷ MS (EI): *m/z* (%): 368 (100) [M]⁺; MS (CI⁺): *m/z* (%): 369 (100) [M+H]⁺; UV/Vis (CHCl₃): λ_{max} = 417 nm; elemental analysis calcd (%) for C₂₀H₁₆O₃ (368.04): C 65.18, H 4.38; found: C 65.11, H 4.42.

Electrochemistry and spectroelectrochemistry: Electrochemical experiments were carried out with a BAS-CV50W electrochemical workstation with positive feedback compensation. Cyclic voltammetry was performed in a three-electrode cell equipped with a platinum disk (Ø 1.6 or 1.0 mm) as working electrode, platinum wire as a counter electrode, and a nonaqueous Ag/Ag⁺ reference electrode (0.01 M AgNO₃ in dry MeCN). The potential of the reference electrode was checked against the ferrocene/ferrocenium couple (Fc/Fc⁺) before and after the experiments, which showed the following average potentials against the reference electrode: +0.079 V (vs. Ag/Ag⁺ in MeCN), +0.130 V (vs. Ag/Ag⁺ in CH₂Cl₂). CVs were recorded in CH₂Cl₂ or MeCN with tetrabutylammonium hexafluorophosphate (Bu₄NPF₆) as a supporting electrolyte. Experiments in MeCN and CH₂Cl₂ were performed in dry HPLC-grade solvents, deoxygenated by Ar bubbling. The CV for compound **8** was measured versus Ag/AgCl reference electrode (Figure S1 in the Supporting Information). Spectroelectrochemical measurements in CH₂Cl₂ and MeCN were performed on a Genesys 10 spectrophotometer in a 1 mm quartz cell using a Pt grid as the working electrode, Pt wire as the counter electrode, and Ag wire as the reference electrode, with 0.2 M (in CH₂Cl₂) or 0.1 M (in MeCN) Bu₄NPF₆ as supporting electrolyte. BAS-CV50W electrochemical workstation was used as a potentiostat in SEC experiments.

UV/Vis/NIR and IR spectra: Electron absorption spectra were recorded on Perkin–Elmer Lambda 900 UV/VIS/NIR spectrophotometer in either 10 mm or 1 mm quartz cells. Solid-state UV/Vis/NIR spectra for CTC were recorded in KBr pellets versus KBr pellet. Infrared spectra of DTef and its CTC with **10** were recorded on Perkin–Elmer 1600 Series FTIR spectrophotometer in KBr pellets.

Electron paramagnetic resonance: EPR spectra were obtained in an X-band spectrometer (Bruker ESP 300 E) equipped with a field-frequency (F/F) lock accessory and built-in NMR Gaussmeter. A rectangular TE102 cavity was used for the measurements. The signal-to-noise ratio of the spectra was increased by accumulation of scans by using the F/F lock accessory to guarantee large field reproducibility. Precautions to avoid undesirable spectral distortions and line broadenings, such as those arising from microwave power saturation and magnetic field over modulation, were also taken into account. To avoid dipolar line broadening from dissolved oxygen, solutions were always carefully degassed with argon. Electrochemical oxidation was performed “in situ” in the spectrometer cavity using a specially designed quartz cell connected to an EG&G Model 263 A Potentiostat/Galvanostat.

X-ray crystallography: X-ray diffraction experiments were carried out on a Bruker three-circle diffractometer with a SMART 6000 CCD area detector, by using graphite-monochromated MoK_α radiation (λ = 0.71073 Å) and a Cryostream (Oxford Cryosystems) open-flow N₂ cryostat. The structure was solved by direct methods and refined by full-matrix least-squares against *F*² of all reflections, by using SHELXTL v. 6.12 software (Bruker AXS, Madison WI, USA, 2001).

Crystal data for 8: C₂₀H₁₆S₃, *M*_r = 352.51, *T* = 120 K, monoclinic, space group *P2₁/n* (No. 14, nonstandard setting), *a* = 9.590(1), *b* = 7.659(1), *c* = 23.140(3) Å, β = 101.06(1)°, *V* = 1668.1(4) Å³, *Z* = 4, ρ_{calcd} = 1.404 g cm⁻³,

μ = 0.44 mm⁻¹, 22899 reflections with 2θ ≤ 60°, 4785 unique, *R*_{int} = 0.041, *R*(*F*) = 0.041 [3833 data with *F*² ≥ 2σ(*F*²)], w*R*(*F*²) = 0.140 (all data).

Crystal data for 10-(DTef)₂-2PhCl: Crystals of **10**-(DTef)₂-2PhCl grew as thin plates, non-merohedrally twinned by about 180° rotation around the *c** axis (= major face normal), and were poor diffractors, giving the mean *I*/σ(*I*) ratio of only 2.1, hence the low precision of the structure. *M*_r = 1536.34, *T* = 120 K, triclinic, space group *P* $\bar{1}$ (No. 2), *a* = 12.678(4), *b* = 15.627(5), *c* = 17.274(5) Å, α = 75.80(1), β = 87.18(1), γ = 83.03(1)°, *V* = 3293(2) Å³, *Z* = 2, ρ_{calcd} = 1.550 g cm⁻³, μ = 0.34 mm⁻¹, 17397 reflections with 2θ ≤ 50°, 11076 unique, *R*_{int} = 0.29, *R*(*F*) = 0.180 [2725 data with *F*² ≥ 2σ(*F*²)], w*R*(*F*²) = 0.446 (all data).

CCDC-298158 (**8**) and CCDC-298159 (**10**-(DTef)₂-2PhCl) contain the supplementary crystallographic data for this paper. These data can be obtained free of charge from The Cambridge Crystallographic Data Centre via www.ccdc.cam.ac.uk/data_request/cif.

Computational procedures: The ab initio computations of molecules **8** and **10** were carried out with the Gaussian 03^[38] package of programs at density-functional theory (DFT) level using Pople's 6-31G or 6-311G split valence basis sets supplemented by one or two *d*-polarization functions on heavy atoms and *p*-polarization functions on hydrogen atoms (or without them). DFT calculations were carried out using Becke's three-parameter hybrid exchange functional^[39] with Lee–Yang–Parr gradient-corrected correlation functional (B3LYP).^[40] Thus, the geometries were optimized with B3LYP/6-31G(d) and the energies and electronic structures were then calculated for single point at the B3LYP/6-311G(2d,p) level. Restricted Hartree–Fock formalism was applied for geometry optimization and electronic structures calculations for neutral, dication, and tetracation states and spin unrestricted formalism was used in the case of radical cations. Contours of HOMO and LUMO orbitals were visualized using Molekel v.4.3 program.^[41] No constraints of bonds/angles/dihedral angles were applied in the calculations and all the atoms were free to optimize.

Acknowledgements

The work in Durham, as part of the European Science Foundation EU-ROCORES Programme NANOSYN, was supported by funds from the EPSRC and the EC 6th Framework Programme.

- [1] a) M. Kozaki, S. Tanaka, Y. Yamashita, *J. Org. Chem.* **1994**, *59*, 442–450; b) N. Martín, E. Ortí, L. Sánchez, P. M. Viruela, R. Viruela, *Eur. J. Org. Chem.* **1999**, 1239–1247; c) B. Halton, C. S. Jones, *Eur. J. Org. Chem.* **2004**, 138–146.
- [2] T. Sugimoto, H. Awaji, Y. Misaki, T. Kawase, S. Yoneda, Z. Yoshida, *Chem. Mater.* **1989**, *1*, 535–547.
- [3] T. K. Hansen, M. V. Lakshminantham, M. P. Cava, R. M. Metzger, J. Becher, *J. Org. Chem.* **1991**, *56*, 2720–2722.
- [4] M. R. Bryce, A. J. Moore, B. K. Tanner, R. Whitehead, W. Clegg, F. Gerson, A. Lambrecht, S. Pfenninger, *Chem. Mater.* **1996**, *8*, 1182–1188.
- [5] Y. Yamashita, M. Tomura, M. B. Zaman, K. Imaeda, *Chem. Commun.* **1998**, 1657–1658.
- [6] A. J. Moore, M. R. Bryce, A. S. Batsanov, A. Green, J. A. K. Howard, M. A. McKervey, P. McGuigan, I. Ledoux, E. Ortí, R. Viruela, P. M. Viruela, B. Tarbit, *J. Mater. Chem.* **1998**, *8*, 1173–1184.
- [7] a) Z. Yoshida, T. Kawase, H. Awaji, I. Sugimoto, T. Sugimoto, S. Yoneda, *Tetrahedron Lett.* **1983**, *24*, 3469–3472; b) M. R. Bryce, M. A. Coffin, W. Clegg, *J. Org. Chem.* **1992**, *57*, 1696–1699.
- [8] a) Z. Yoshida, T. Kawase, H. Awaji, S. Yoneda, *Tetrahedron Lett.* **1983**, *24*, 3473–3476; b) A. J. Moore, M. R. Bryce, *Tetrahedron Lett.* **1992**, *33*, 1373–1376.
- [9] For extended TTFs with alkynyl spacers see: a) A. Khanous, A. Gorgues, M. Jubault, *Tetrahedron Lett.* **1990**, *31*, 7311–7314; b) M. B. Nielsen, N. N. P. Moonen, C. Boudon, J.-P. Gisselbrecht, P. Seiler, M. Gross, F. Diederich, *Chem. Commun.* **2001**, 1848–1849;

- c) M. B. Nielsen, N. F. Utesch, N. N. P. Moonen, C. Boudon, J.-P. Gisselbrecht, S. Concilio, S. P. Piotto, P. Seiler, P. Günter, M. Gross, F. Diederich, *Chem. Eur. J.* **2002**, *8*, 3601–3613.
- [10] N. Bellec, K. Boubekeur, R. Carlier, P. Hapiot, D. Lorcy, A. Tallec, *J. Phys. Chem. A* **2000**, *104*, 9750–9759.
- [11] a) D. Lorcy, R. Carlier, A. Robert, A. Tallec, P. Le Maguerès, L. Ouahab, *J. Org. Chem.* **1995**, *60*, 2443–2447; b) P. Hapiot, D. Lorcy, A. Tallec, R. Carlier, A. Robert, *J. Phys. Chem.* **1996**, *100*, 14823–14827.
- [12] M. Guerro, D. Lorcy, *Tetrahedron Lett.* **2005**, *46*, 5499–5502.
- [13] a) K. Hu, D. H. Evans, *J. Phys. Chem.* **1996**, *100*, 3030–3036; b) N. A. Macías-Ruvalcaba, D. H. Evans, *J. Phys. Chem. B*, **2005**, *109*, 14642–14647.
- [14] A. J. Moore, M. R. Bryce, P. J. Skabara, A. S. Batsanov, L. M. Goldenberg, J. A. K. Howard, *J. Chem. Soc. Perkin Trans. 1* **1997**, 3443–3449.
- [15] Y. Misaki, Y. Matsumura, T. Sugimoto, Z. Yoshida, *Tetrahedron Lett.* **1990**, *31*, 5289–5292.
- [16] a) M. A. Coffin, M. R. Bryce, A. S. Batsanov, J. A. K. Howard, *J. Chem. Soc. Chem. Commun.* **1993**, 552–554; b) M. R. Bryce, M. A. Coffin, P. J. Skabara, A. J. Moore, A. S. Batsanov, J. A. K. Howard, *Chem. Eur. J.* **2000**, *6*, 1955–1962.
- [17] R. R. Amaresh, D. Liu, T. Konovalova, M. V. Lakshmikantham, M. P. Cava, L. D. Kispert, *J. Org. Chem.* **2001**, *66*, 7757–7764.
- [18] M. Kluba, J. Harwood, P. K. Casey, A. L. Ternay, *J. Heterocycl. Chem.* **1985**, *22*, 1261–1267.
- [19] A. J. Moore, M. R. Bryce, *J. Chem. Soc. Perkin Trans. 1* **1991**, 157–168.
- [20] M. R. Bryce, T. Finn, A. J. Moore, A. S. Batsanov, J. A. K. Howard, *Eur. J. Org. Chem.* **2000**, 51–60.
- [21] a) M. R. Bryce, M. A. Coffin, M. B. Hursthouse, A. I. Karaulov, K. Müllen, H. Scheich, *Tetrahedron Lett.* **1991**, *32*, 6029–6032; b) N. Martín, L. Sánchez, C. Seoane, E. Ortí, P. M. Viruela, R. Viruela, *J. Org. Chem.* **1998**, *63*, 1268–1279; c) I. Pérez, S.-G. Liu, N. Martín, L. Echegoyen, *J. Org. Chem.* **2000**, *65*, 3796–3803; d) D. F. Perepichka, M. R. Bryce, I. F. Perepichka, S. B. Lyubchik, C. A. Christensen, N. Godbert, A. S. Batsanov, E. Levillain, E. J. L. McInnes, J. P. Zhao, *J. Am. Chem. Soc.* **2002**, *124*, 14227–14238.
- [22] M. Guerro, R. Carlier, K. Boubekeur, D. Lorcy, P. Hapiot, *J. Am. Chem. Soc.* **2003**, *125*, 3159–3167.
- [23] This nomenclature is clarified by the depicted structures of *trans*- and *cis*-**10**. Whereas both structures are not planar, the orientation of the dithiole moieties in the optimized geometries are denoted as *cis* or *trans* with respect to C(a)–C(b) bond of the =CH–CH= fragment (see the Supporting Information). In the neutral state this nomenclature is not strictly correct as this is formally a single bond: *syn* and *anti* could be used. However, in the dication state the double –Ca=Cb– bond allows clear assignment of *cis* and *trans* isomers.
- [24] a) P. Hascoat, D. Lorcy, A. Robert, R. Carlier, A. Tallec, K. Boubekeur, P. Batail, *J. Org. Chem.* **1997**, *62*, 6086–6089; b) S. González, N. Martín, L. Sánchez, J. L. Segura, C. Seoane, I. Fonseca, F. H. Cano, J. Sedó, J. Vidal-Gancedo, C. Rovira, *J. Org. Chem.* **1999**, *64*, 3498–3506.
- [25] D. F. Perepichka, M. R. Bryce, E. J. L. McInnes, J. P. Zhao, *Org. Lett.* **2001**, *3*, 1431–1434.
- [26] a) I. F. Perepichka, L. G. Kuz'mina, D. F. Perepichka, M. R. Bryce, L. M. Goldenberg, A. F. Popov, J. A. K. Howard, *J. Org. Chem.* **1998**, *63*, 6484–6493; b) I. F. Perepichka, A. F. Popov, T. V. Orekhova, M. R. Bryce, A. M. Andrievskii, A. S. Batsanov, J. A. K. Howard, N. I. Sokolov, *J. Org. Chem.* **2000**, *65*, 3053–3063.
- [27] a) A. J. Moore, M. R. Bryce, A. S. Batsanov, J. N. Heaton, C. W. Lehmann, J. A. K. Howard, N. Robertson, A. E. Underhill, I. F. Perepichka, *J. Mater. Chem.* **1998**, *8*, 1541–1550; b) A. S. Batsanov, M. R. Bryce, A. Chesney, J. A. K. Howard, D. E. John, A. J. Moore, C. L. Wood, H. Gershtenman, J. Y. Becker, V. Y. Khodorkovsky, A. Ellern, J. Bernstein, I. F. Perepichka, V. Rotello, M. Gray, A. O. Cuello, *J. Mater. Chem.* **2001**, *11*, 2181–2191; c) L. G. Kuz'mina, I. F. Perepichka, D. F. Perepichka, J. A. K. Howard, M. R. Bryce, *Kristallografiya* **2002**, *47*, 286–296; *Crystallogr. Rep.* **2002**, *47*, 251–261.
- [28] S. Horiuchi, H. Yamochi, G. Saito, K. Sakaguchi, M. Kusunoki, *J. Am. Chem. Soc.* **1996**, *118*, 8604–8622.
- [29] I. F. Perepichka, Z. V. Stepanenko, E. Levillain, I. M. Serebraykov, Y. Sahin, unpublished results.
- [30] J. Silverman, N. F. Yannoni, A. P. Krukoni, *Acta Crystallogr. Sect. B* **1974**, *30*, 1474–1480.
- [31] a) R. E. Del Sesto, J. S. Miller, P. Lafuente, J. J. Novoa, *Chem. Eur. J.* **2002**, *8*, 4894–4908; b) J.-M. Lü, S. V. Rosokha, J. K. Kochi, *J. Am. Chem. Soc.* **2003**, *125*, 12161–12171, and references therein.
- [32] D. D. Mysyk, I. F. Perepichka, N. I. Sokolov, *J. Chem. Soc. Perkin Trans. 2* **1997**, 537–545.
- [33] V. F. Kaminskii, R. P. Shibaeva, L. O. Atovmyan, *Zh. Strukt. Khim.* **1974**, *15*, 509 (in Russian).
- [34] Metallic type conductivity ($\sigma_n = 18 \text{ Scm}^{-1}$, $\sigma_{\text{max}} = 36 \text{ Scm}^{-1}$ at 94 K) of BEDO–DTeF, 2:1 CTC (BEDO is bis(ethylenedioxy)tetrathiafulvalene) suggests segregated stacks of the donor and the acceptor in the complex, although no single-crystal X-ray diffraction structure has been reported.^[28] Segregated stacking is, of course, a common motif in TTF–TCNQ type complexes; it was observed before in the TTF–TCNQ complex, with the minimum TCNQ–TCNQ separation of 3.090 Å: a) A. J. Schultz, G. D. Stucky, R. H. Blessing, P. Coppens, *J. Am. Chem. Soc.* **1976**, *98*, 3194–3198; b) D. Jerome, *Chem. Rev.* **2004**, *104*, 5565–5591.
- [35] S. Amriou, C. Wang, A. S. Batsanov, M. R. Bryce, D. F. Perepichka, E. Ortí, R. Viruela, J. Vidal-Gancedo, C. Rovira, *Chem. Eur. J.* **2006**, *12*, 3389–3400.
- [36] F. H. Allen, O. Kennard, D. G. Watson, L. Brammer, A. G. Orpen, *J. Chem. Soc. Perkin Trans. 2* **1987**, S1–S19.
- [37] The existence of compound **12** as two isomers is clear from its ¹H NMR spectrum and results in a complicated ¹³C NMR spectrum. Some sp² carbon signals in the high-field ¹³C NMR spectrum appear as separate peaks for two isomers, whereas others are equivalent or overlapped. Therefore, the total number of observed carbon signals is an intermediate value between the single structure and two isomeric structures. Similar behavior was also observed for compound **13**.
- [38] Gaussian 03, Revision B.04, M. J. Frisch, G. W. Trucks, H. B. Schlegel, G. E. Scuseria, M. A. Robb, J. R. Cheeseman, J. A. Montgomery, Jr., T. Vreven, K. N. Kudin, J. C. Burant, J. M. Millam, S. S. Iyengar, J. Tomasi, V. Barone, B. Mennucci, M. Cossi, G. Scalmani, N. Rega, G. A. Petersson, H. Nakatsuji, M. Hada, M. Ehara, K. Toyota, R. Fukuda, J. Hasegawa, M. Ishida, T. Nakajima, Y. Honda, O. Kitao, H. Nakai, M. Klene, X. Li, J. E. Knox, H. P. Hratchian, J. B. Cross, V. Bakken, C. Adamo, J. Jaramillo, R. Gomperts, R. E. Stratmann, O. Yazyev, A. J. Austin, R. Cammi, C. Pomelli, J. W. Ochterski, P. Y. Ayala, K. Morokuma, G. A. Voth, P. Salvador, J. J. Dannenberg, V. G. Zakrzewski, S. Dapprich, A. D. Daniels, M. C. Strain, O. Farkas, D. K. Malick, A. D. Rabuck, K. Raghavachari, J. B. Foresman, J. V. Ortiz, Q. Cui, A. G. Baboul, S. Clifford, J. Cioslowski, B. B. Stefanov, G. Liu, A. Liashenko, P. Piskorz, I. Komaromi, R. L. Martin, D. J. Fox, T. Keith, M. A. Al-Laham, C. Y. Peng, A. Nanayakkara, M. Challacombe, P. M. W. Gill, B. Johnson, W. Chen, M. W. Wong, C. Gonzalez, J. A. Pople, Gaussian, Inc., Wallingford CT, **2004**.
- [39] a) A. D. Becke, *Phys. Rev. A* **1988**, *38*, 3098–3100; b) A. D. Becke, *J. Chem. Phys.* **1993**, *98*, 5648–5652.
- [40] C. Lee, W. Yang, R. G. Parr, *Phys. Rev. B* **1988**, *37*, 785–789.
- [41] a) P. Flükiger, H. P. Lüthi, S. Portmann, J. Weber, Molekel, Version 4.3, Swiss Center for Scientific Computing, Manno (Switzerland), **2002**, <http://www.cscs.ch/molekel/>; b) S. Portmann, H. P. Lüthi, *Chimia* **2000**, *54*, 766–769.

Received: February 21, 2006
Published online: May 23, 2006